Title

Rab25-Mediated EGFR Recycling Causes Tumor Acquired Radioresistance

Journal

iScience, 23(4)

ISSN

2589-0042

Authors

Zhang, Lu
Xie, Bowen
Qiu, Yanfang
et al.

Publication Date

2020-04-01

DOI

10.1016/j.isci.2020.100997

Peer reviewed

iScience

CellPress

Article

Rab25-Mediated EGFR Recycling Causes Tumor Acquired Radioresistance

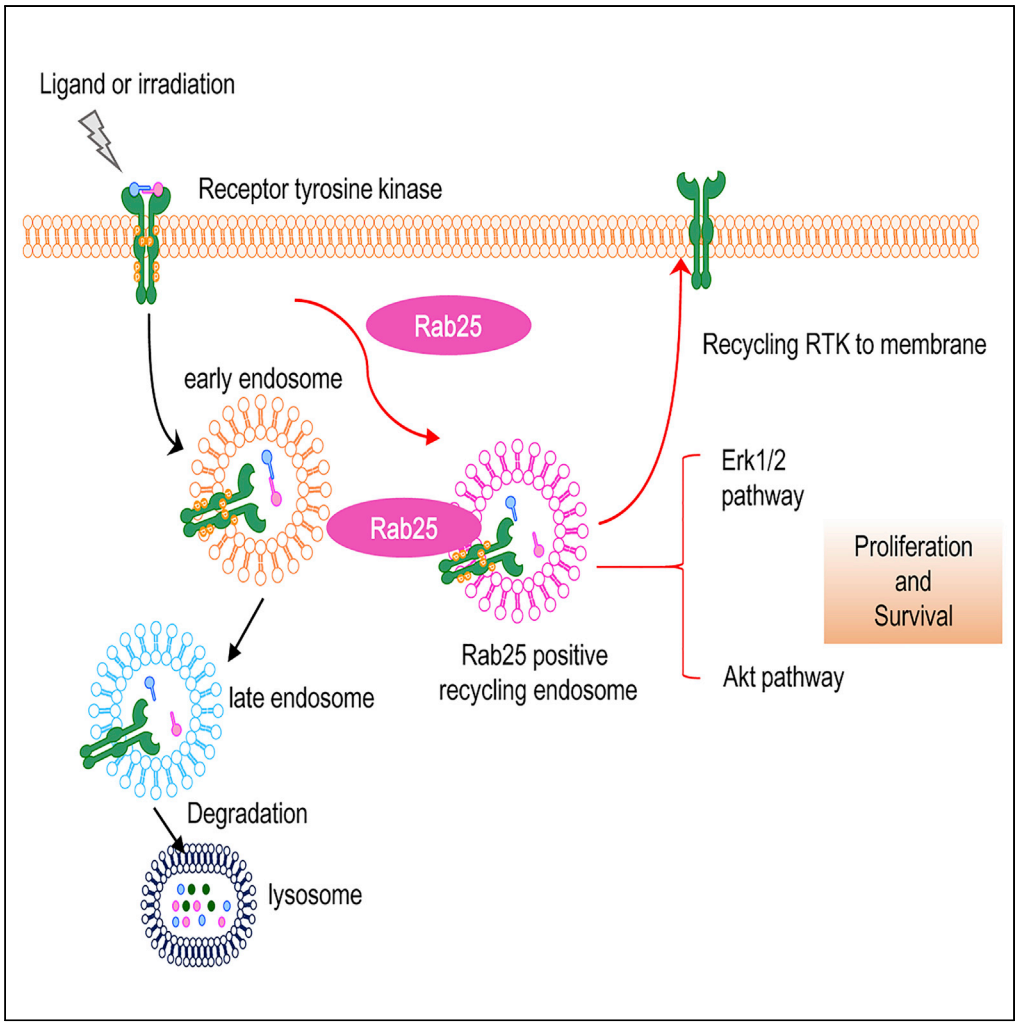

Lu Zhang, Bowen Xie, Yanfang Qiu, ..., Rong Tan, Jian Jian Li, Lun-Quan Sun

jijli@ucdavis.edu (J.J.L.)
lunquansun@csu.edu.cn (L.-Q.S.)

HIGHLIGHTS

High expression of Rab25 is linked to radioresistance and EMT in lung cancer and NPC

Rab25 promotes cell therapeutic resistance via RTK-mediated signaling pathways

Rab25 elevates EGFR recycling rate onto the membrane in therapeutic-resistant cells

Targeting Rab25 combined with IR might be a potent treatment for the patients with cancer

Zhang et al., iScience *23*, 100997
April 24, 2020
https://doi.org/10.1016/j.isci.2020.100997

iScience

CellPress

Article

Rab25-Mediated EGFR Recycling Causes Tumor Acquired Radioresistance

Lu Zhang,[1,2,3] Bowen Xie,[1,2,3] Yanfang Qiu,[1] Di Jing,[1,3] Jing Zhang,[1] Yumei Duan,[4] Zhi Li,[1,2] Ming Fan,[3] Jiang He,[1,2] Yuanzheng Qiu,[5] Rong Tan,[1,2] Jian Jian Li,[3,6,*] and Lun-Quan Sun[1,2,7,8,*]

SUMMARY

Tumor acquired radioresistance remains as the major limit in cancer radiotherapy (RT). Rab25, a receptor recycling protein, has been reported to be enhanced in tumors with aggressive phenotype and chemotherapy resistance. In this study, elevated Rab25 expression was identified in an array of radioresistant human cancer cell lines, *in vivo* radioresistant xenograft tumors. Clinical investigation confirmed that Rab25 expression was also associated with a worse prognosis in patients with lung adenocarcinoma (LUAD) and nasopharyngeal carcinoma (NPC). Enhanced activities of EGFR were observed in both NPC and LUAD radioresistant cells. Rab25 interacts with EGFR to enhance EGFR recycling to cell surface and to decrease degradation in cytoplasm. Inhibition of Rab25 showed synergized radiosensitivity with reduced aggressive phenotype. This study provides the clinical and experimental evidence that Rab25 is a potential therapeutic target to alleviate the hyperactive EGFR signaling and to prevent RT-acquired tumor resistance in patients with LUAD and NPC.

INTRODUCTION

More than 50% of solid tumors including lung adenocarcinoma (LUAD) and nasopharyngeal carcinoma (NPC) are treated by radiotherapy (RT). However, to enhance the RT efficacy it remains urgent to invent effective targets to eliminate the acquired resistance in treated tumor cells (Huang et al., 2013; Aravindan et al., 2014; Begg et al., 2011). Among the major signaling pathways dominated in cancer cells, the activation of receptor tyrosine kinases (RTKs) has been identified to be the most frequent oncogenic event that drives proliferation and malignant phenotype in tumor cells (Casaletto and Mcclatchey, 2012) and the activated EGFR is tightly associated with tumor response and prognosis after RT (Jakobsen et al., 2016; Higgins et al., 2016). Targeting RTK suppresses tumor growth and synergizes the efficacy of RT (Camidge et al., 2014). Although recycling of EGFR via endosomal pathway is able to enhance oncogenic potency and tumor aggressive phenotype (Shapira et al., 2013; Ye et al., 2016), the mechanism of EGFR recycling underlying tumor adaptive radioresistance remains unsolved.

Both the endocytosis and recycling of EGFR could be enhanced when it is combined with its ligand EGF or under stress condition (Ceresa, 2012; Tan et al., 2016). However, it is unclear how the two processes are coordinated in EGFR-targeted therapy using small molecule tyrosine kinase inhibitors (TKIs) or EGFR-specific antibodies (Chung et al., 2011; Ricordel et al., 2018). To treat tumors with the acquired resistance to TKIs, RT among the others is a choice especially for treatment of local lesions. It has been identified that after endocytosis, the ligand-bound EGFR is arrested in the endosomes via p38/MAPK, which has been linked with the cell death induced by UV, TNFα, or cisplatin (Zwang and Yarden, 2006; Tomas et al., 2015). However, the mechanism regulating the traffic and recycling of EGFR in RT-induced tumor adaptive resistance remains elusive.

Rab25, a member of the Rab11 family, predominantly expresses in epithelial cells and plays a key role in recycling of endosome compartment (Hehnly and Doxsey, 2014). Enhanced GTPase activity is detected in Rab25 compared with other recycling-endosome-related Rab proteins (Casanova et al., 1999). Accumulating evidence suggests that Rab25 is actively involved in carcinogenesis and aggressive phenotype of tumors (Cheng et al., 2012; Dozynkiewicz et al., 2012) and inhibition of Rab25 reduces the aggressive growth in cancer cells (Mitra et al., 2017). Integrin α5β1 is reported to transport by Rab25-positive endosome (Caswell et al., 2007). Rab25 collaborated with CLIC3 to recycle α5β1 in cells of pancreatic ductal adenocarcinoma to promote tumor aggression (Dozynkiewicz et al., 2012). Although both Rab25 and EGFR are suggested to be involved in tumor response to therapies with gefitinib and migration (Jeong et al., 2018; Jo et al., 2014), the interplay between these two factors in signaling tumor acquired radioresistance is to be investigated.

[1]Center for Molecular Medicine, Xiangya Hospital, Central South University, Changsha 410008, China

[2]Key Laboratory of Molecular Radiation Oncology of Hunan Province, Changsha 410008, China

[3]Department of Radiation Oncology, University of California Davis, Sacramento, CA 95817, USA

[4]Department of Pathology, Xiangya Hospital, Central South University, Changsha 410008, China

[5]Department of Otolaryngology Head and Neck Surgery, Xiangya Hospital, Central South University, Changsha 410008, China

[6]NCI-desginaged Comprehensive Cancer Center, Sacramento, CA 95817, USA

[7]National Clinical Research Center for Geriatric Disorders Xiangya Hospital, Changsha, China 410008

[8]Lead Contact

*Correspondence: jijli@ucdavis.edu (J.J.L.), lunquansun@csu.edu.cn (L.-Q.S.)

https://doi.org/10.1016/j.isci.2020.100997

Using radioresistant tumor models from two human cancers mostly treated by RT, this study revealed a previously unknown mechanism by which Rab25 enhances the aberrant transportation of EGFR in radiation-adapted cancer cells. Rab25 is overexpressed in the radioresistant cancer cells and in radioresistant xenograft tumors treated by *in vivo* RT and correlated with poorer RT response and disease-free survival rate. High expression of Rab25 in the radioresistant cells enhanced the transportation of EGFR to cell surface upon ligand stimulation, and blockage of Rab25 reduced the clonogenicity and aggressive phenotype of radioresistant cancer cells. These provide the evidence indicating that Rab25 plays a critical role in radiation-induced aberrant transportation of EGFR, and thus the Rab25-EGFR pathway is a potential therapeutic target to re-sensitize radioresistant cancer cells.

RESULTS

Rab25 Is Correlated with Tumor Response to RT

To identify key factors associated with NPC radioresistance, a profile of 84 cell death-related genes (Qiagen) was analyzed in CNE2R versus its wild-type counterpart CNE2 (Guo et al., 2003; Li et al., 2013; Fu et al., 2019). This pair of cells showed different morphology, EMT potential, and radiation-induced apoptotic cell death (Figures S1A–S1C). Among the short list of genes upregulated in radioresistant NPC cell CNE2R, Rab25, the only protein involved in cargo recycling, showed a 7-fold increase in comparison with CNE2 cells (Figure S1D). The enhanced Rab25 protein levels were then further identified in CNE2R and in three radioresistant LUAD (A549R, H358R, and H157R) cells You et al., 2014 (Figure 1A) and two chemo-resistant cancer cell lines, ovarian cancer SKOV3R and NPC CNE1-TR cells Hou et al., 2017; Zhang et al., 2012; Zhou et al., 2015 (Figure S3A). We also observed a significant increased expression of Rab25 in lung xenografts that received one dose of radiation (Figure 1B), suggesting that radiation might induce Rab25 expression.

To elucidate why expression of Rab25 could be induced by a single dose of radiation, we assume that such a quick induction of Rab25 expression may well be mediated at a transcriptional level. Thus, we sought candidate transcriptional factors in the 500-bp promoter region of Rab25 gene by a prediction database JASPAR (http://jaspar.genereg.net/) and found that there were two binding sites of Stat5 in the promoter of Rab25 (Figure S1E). As reported by us (Fu et al., 2019) and others (Hasselbach et al., 2005; Maranto et al., 2018), STAT5 is one of the important transcriptional factors responsive to irradiation. In CNE2R cells, expression of Stat5a or Stat5b was much higher than in CNE2 cell and could be induced by a single dose of radiation (Figures S1F and S1G). We also observed an induction for protein levels of both Rab25 and Stat5 in CNE2 cell after a single-dose radiation (Figure S1H). Knockdown of Stat5a and Stat5b by small interfering RNA (siRNA) in CNE2R cell dramatically decreased the expression of Rab25 (Figure S1I). The above results suggested that Stat5 might be an important transcriptional factor for Rab25 and might regulate the radiation-induced expression of Rab25.

We constructed a radioresistant xenografts model to study whether Rab25 expression is linked to radioresistance *in vivo*. Briefly, we injected CNE2 cells subcutaneously into the flank of nude mice (P0), and when xenografts volume reached 200 mm^3, we passaged the xenograft into another mice (P1). From P1 passage, xenografts were irradiated at 5 Gy two times when their volume reached 200 mm^3. Xenografts had received a total dose of 110 Gy when we transplanted tumor for 11 passages (Figure 1C). Compared with P1 (only transplant for one passage), P11 tumor growth became non-responsive to radiotherapy after 5 Gy*2 treatments (Figure S2A). The enhanced Rab25 immunohistochemistry (IHC) staining was observed in three of four P11 xenografts, whereas no enhanced IHC staining was detected in four P0 xenografts, demonstrating that Rab25 can be up-regulated in tumors that received radiotherapy *in vivo*, or in other words, Rab25 was enhanced in radioresistant tumors (Figures 1D). In addition, the Rab25 IHC staining in sham P4 tumor (just transplanted for four passages without irradiation) was not increased, suggesting that transplantation alone might not induce Rab25 expression (Figure S2B).

To further examine Rab25-mediated tumor aggressive phenotype, IHC staining of Rab25 was conducted on 101 tumor tissues of patients with NPC who received upfront standard radiotherapy in Xiangya Hospital in recent 5 years. According to the treatment outcomes evaluated using magnetic resonance imaging (MRI) and the Response Evaluation Criteria in Solid Tumors (RECIST) used in the clinic, patients were categorized into three groups: complete response (CR), partial response (PR), and stable disease (SD). Rab25 expression was then evaluated in these three groups. All 17 SD samples (100%) and 33 of 47 (70.2%) PR samples showed strong Rab25 staining, whereas only 8 of 37 (21.6%) of the CR samples were Rab25 positive (score higher than 2, Figures 2A and S2C). However, Rab25 expression was not significantly correlated with

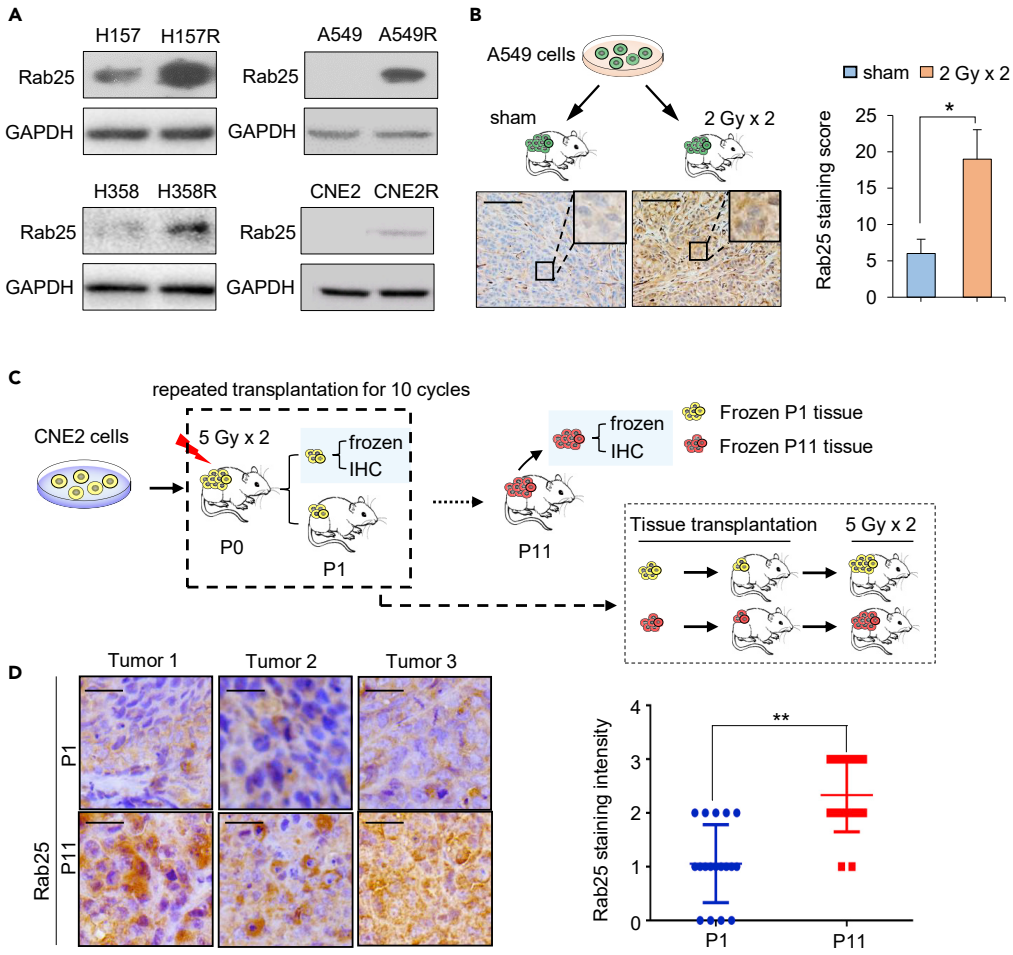

Figure 1. Induction of Rab25 Is Involved in Acquired Tumor Radioresistance

(A) Increased Rab25 expression in radioresistant lung cancer cells (H157R, H358R, and A549R) and NPC cells (CNE2R) derived from the surviving residues of corresponding wild-type counterparts treated by radiation with fractionated doses.

(B) Schematic (top) and IHC staining of Rab25 in A549 xenografts treated with or without local irradiation, 2 Gy per day for 2 days (bottom). The average Rab25-positive cells in tumors were quantified and are shown in the right bar graph. Scale bar, 50 μm. n = 3, mean ± SD, *p < 0.05.

(C) Schematic diagram for establishment of radioresistant xenograft model. CNE2 cells were injected subcutaneously into the right flanks of nude mice, and when tumors reached a volume of approximately 200 mm^3, radiotherapy was delivered to the local tumor (5 Gy per day for 2 days; total dose = 10 Gy). On day 5 after last irradiation, the tumors were removed and one part of tumor tissues was fixed for IHC analysis and another part of tumor tissues was inoculated subcutaneously into the right flank of another mouse (P1). When the volume of the re-planted tumors in the P1 mice reached approximately 200 mm^3, radiotherapy was delivered again with the same dose, and such treatment was repeated for 11 cycles (P11). The radiosensitivity of tumors from P1 and P11 mice was measured by transplanting the tumors from P1 and P11 mice and irradiating with 5 Gy × 2 when tumor reached 200 mm^3.

(D) Representative IHC staining of Rab25 in P1 and P11tumors (left). The average Rab25-positive cells in tumors were quantified (six fields were randomly selected for each xenograft) and shown in the right. Scale bar, 50 μm. n = 18, mean ± SD, **p < 0.01.

histological stage, lymph node metastasis, age, or tumor size (Table S1), further suggesting that Rab25 is a potential biomarker for predicting the radiotherapy response. An analysis based on the Cancer Genome Atlas (TCGA) revealed that Rab25 is highly expressed in various tumors (Figure 2B and Table S2), including LUAD, which exhibits much higher expression of Rab25 than adjacent normal tissues (Figure 2B). The data from TCGA showed that both overall survival (OS) and disease-free survival (DFS) of the patients with LUAD with high Rab25 expression had worse outcomes than those with low Rab25 expression (Figures 2C and 2D), which suggested a role of Rab25 in tumor progression and therapeutic response.

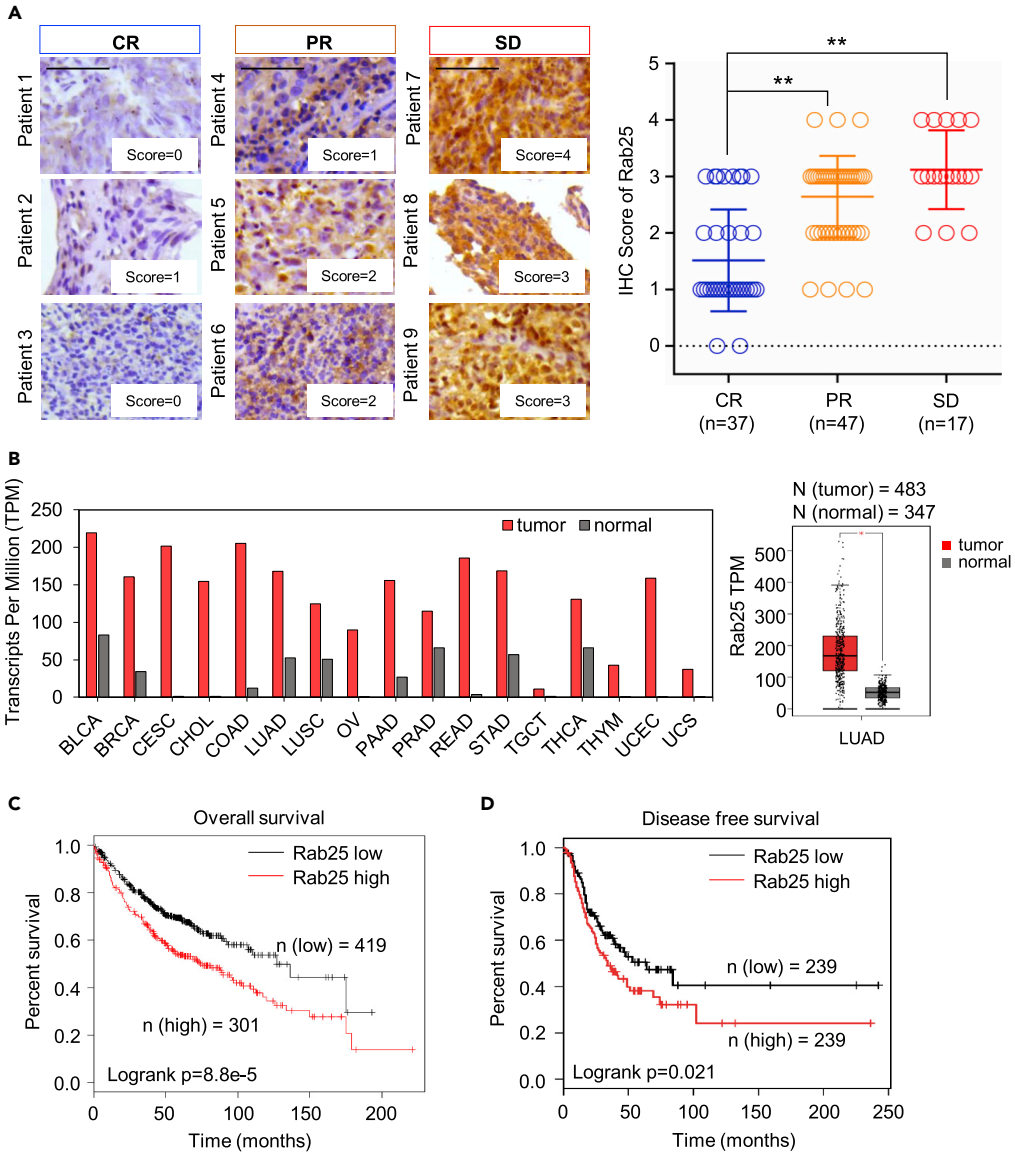

Figure 2. Rab25 Is Linked with Poor Prognosis and Less Responsiveness of Patients with NPC to Radiotherapy

(A) RT responsiveness of 101 patients with NPC was correlated with Rab25 expression levels; clinic response of all patients was scored as complete response (CR), partial response (PR), and stable disease (SD), and expression levels of Rab25 were scored with four levels (0–4) illustrated in left. Scale bar, 50 μm. (B) Elevated Rab25 expression in a large scale of human cancers (red) compared with normal tissues (gray). The graph was generated from the GEPIA website (http://gepia.cancer-pku.cn/) and was based on the transcriptional level of Rab25 in an array of human cancer from multiple cohorts of TCGA study. The median expression of Rab 25 presented as transcripts per million (TPM) was chosen in each cancer type, and the case number of each cancer type was illustrated in Table S2. Right, Rab25 expression summarized from 483 patients with LUAD and 347 normal lung tissues (mean ± SD, *$p < 0.05$). (C) Overall survival or (D) disease-free survival of patients with LUAD generated using the log rank test based on Rab25 expression in LUAD tissues from the TCGA cohort.

Down-Expression of Rab25 Suppresses RTKs-Mediated Signaling Pathways

RTK-mediated signaling is among the most frequently activated pathways that regulate cancer progression and therapeutic response. We observed that the content of EGFR was increased in radio- or chemo-resistant cells, whereas the downstream pathways, including Akt and Erk signaling, were hyperactive (Figures 3A and S3A). In NPC clinical samples, the EGFR expression level and the treatment response were closely correlated in CR and SD groups (Figures 3B and S3B), whereas the levels of EGFR and Rab25 expression

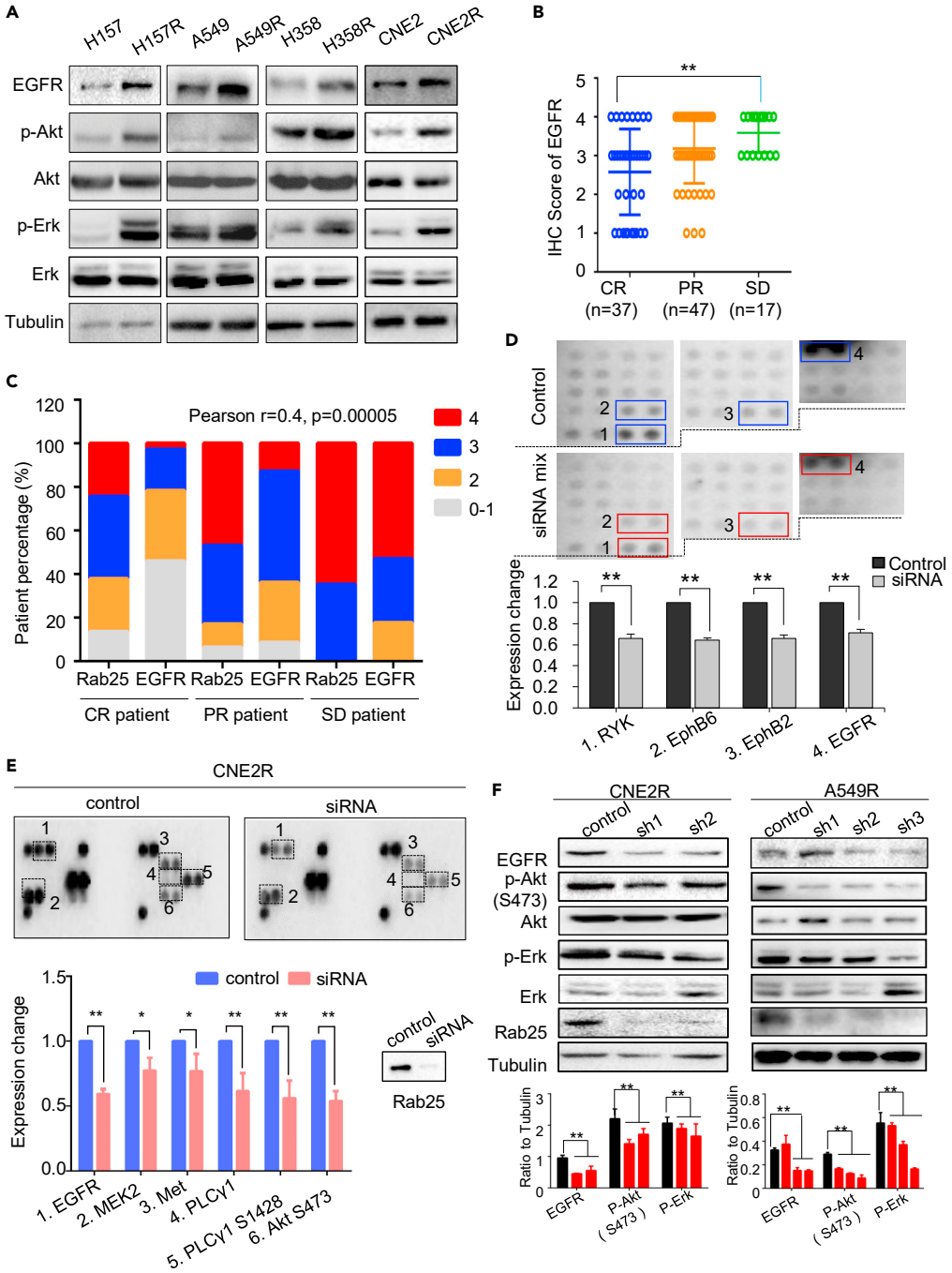

Figure 3. Rab25 Is Involved in the Activation of EGFR Pathway

(A) Immunoblotting of EGFR and phosphorylation status of Akt at Ser^{473} and Erk at Thr^{202} and Tyr^{204} in three pairs of lung radioresistant cells.

(B) Scores of EGFR IHC staining were shown as percentage for EGFR IHC analysis with 4 as the highest and 0 the lowest expression. Representative IHC imaging were shown in Figure S3B.

(C) Co-expression of Rab25 and EGFR in 101 NPC tissues corresponding to the patients grouped as CR, PR, and SD. The intensity of IHC staining is scored from 0 to 1 (for "no signal") to 4 (for "strongest signal"). Rab25 and EGFR staining intensity from each patient was compared as two datasets in a column table. R value was calculated using GraphPad Prism software and the p value was calculated by two-tailed analysis and confidence interval is 95%.

(D) The relative phosphorylation of RTKs in H358R cells and H358R transfected with siRab25. Total proteins were extracted and screened simultaneously using R&D Systems Human Phospho-Receptor Tyrosine Kinase (RTK) Array Kit. The spot

Figure 3. *Continued*

intensities were quantified using ImageJ software. The values for control cells (blue box) were set as 1, and the values of siRab25 (red box) were shown relative to the control, n = 3, mean ± SD, **p < 0.01.

(E) Expression of phosphorylated EGFR, HER2, c-Met, and the associated downstream signal molecules was analyzed by PathScan RTK signaling antibody array kit in CNE2R cell (control) and CNE2R transfected with Rab25 siRNA. The spot intensities were quantified using ImageJ software. The values for control cells (blue) were set as 1, and the values of siRNA (red) were shown relative to the control. Results represent mean ± SD for three analysis. *p < 0.05, **p < 0.01.

(F) Down-expression of Rab25 reduced the expression of EGFR and the activation of associated signaling pathways in radioresistant cells.

was positively associated, indicating these two molecules contributed to NPC radioresponse (Pearson r = 0.4, p = 0.00005; Figure 3C).

Previous studies (Caswell et al., 2007) and our current data demonstrated that Rab25 could regulate the cellular anti-anoikis ability controlled by RTK-mediated signaling. Thus, we suspected that Rab25 might regulate activities of RTKs and their downstream signaling pathways. In radioresistant cells with silenced Rab25, protein array analyses showed that the levels of some RTK molecules, including RYK, EphB6, EphB2, and Met, had significantly decreased (Figures 3D, 3E, S3C) and the downstream signaling activation was inhibited after Rab25 suppression in CNE2R cells (Figure 3E). Furthermore, a decrease in not only EGFR content but also components of the downstream signaling pathways was verified in NPC CNE2R cell and LUAD A549R cell (Figure 3F).

Rab25 Is Involved in Endosomes Transport of EGFR

We wondered that Rab25 may play a key role in signaling radioresistance via EGFR transportation. Using structured illumination microscopy (SIM) super resolution technology, we observed several red circles (represents Rab25 positive endosome) contained green dots (represents EGFR molecule) and red dots were co-localized with green dots (Figure 4A). We then carried out an immunoprecipitation assay using anti-Rab25 antibody in CNE2R cells and observed the association between Rab25 and EGFR (Figure 4B). To further validate their association, we performed Duolink *in situ* proximity ligation assay (PLA) and detected numerous EGFR/Rab25 interaction signals representing Rab25 in close proximity to EGFR. The signals for co-localization (red dots) were enhanced at 1 h post irradiation, suggesting radiation promoted the interactions between Rab25 and EGFR (Figure 4C).

To characterize the effect of Rab25-positive endosomes on EGFR intracellular endosome distribution, we analyzed the co-localization rate of EGFR with early endosome marker EEA1 in radioresistant cells after downregulating Rab25. Rab25 knockdown led to a significant reduction of EGFR in EEA1-positive early endosomes (Figures 4D and 4E), implying that Rab25 might prevent EGFR degradation by routing EGFR to EEA1-positive early endosomes. Consistently, when treating cells with cycloheximide (CHX) to inhibit EGFR synthesis, we observed that the half-life of EGFR was shortened in Rab25-depleted cells (Figure 4F). These results suggest that Rab25-positive endosomes transport EGFR away from late endosomes to prevent its degradation and to maintain active signaling.

Rab25 Transports EGFR onto the Cell Surface upon EGF Stimulation

Next, we examined whether high expression of Rab25 could enhance the membrane content of EGFR. The radioresistant cancer cells exhibited higher level of EGFR on cell surface than that on parental cells (Figure 5A), and EGFR immunostaining of Rab25-knockdown CNE2R cells showed that Rab25 knockdown caused significant reduction of membrane distribution of EGFR (Figure S4A). Then we tracked the membrane content of EGFR at different times after stimulating cell with EGF. The membrane content of EGFR in CNE2R or A549R cells was consistently much higher than that in parental cells after EGF stimulation (Figure 5B). In addition, overexpression or knockdown of Rab25 markedly impacted the tyrosine phosphorylation of EGFR (Figures 5C and 5D), further indicating that Rab25 influenced EGFR activity.

To clarify whether membrane content alteration of EGFR mediated by Rab25 was on account of the variation in ligand-induced endocytosis, we stimulated cells with two doses of Alexa Fluor 488-EGF (1 or 100 ng/mL) to monitor EGF uptake in CNE2R cells with or without Rab25 knockdown. Flow cytometry analysis showed that, regardless of the EGF concentration, no difference of the rate of EGF uptake was observed between the two types of cells, indicating that Rab25-mediated regulation of the membrane EGFR content was not due to a variation in the coated vesicle formation rate (Figure 5E). The membrane

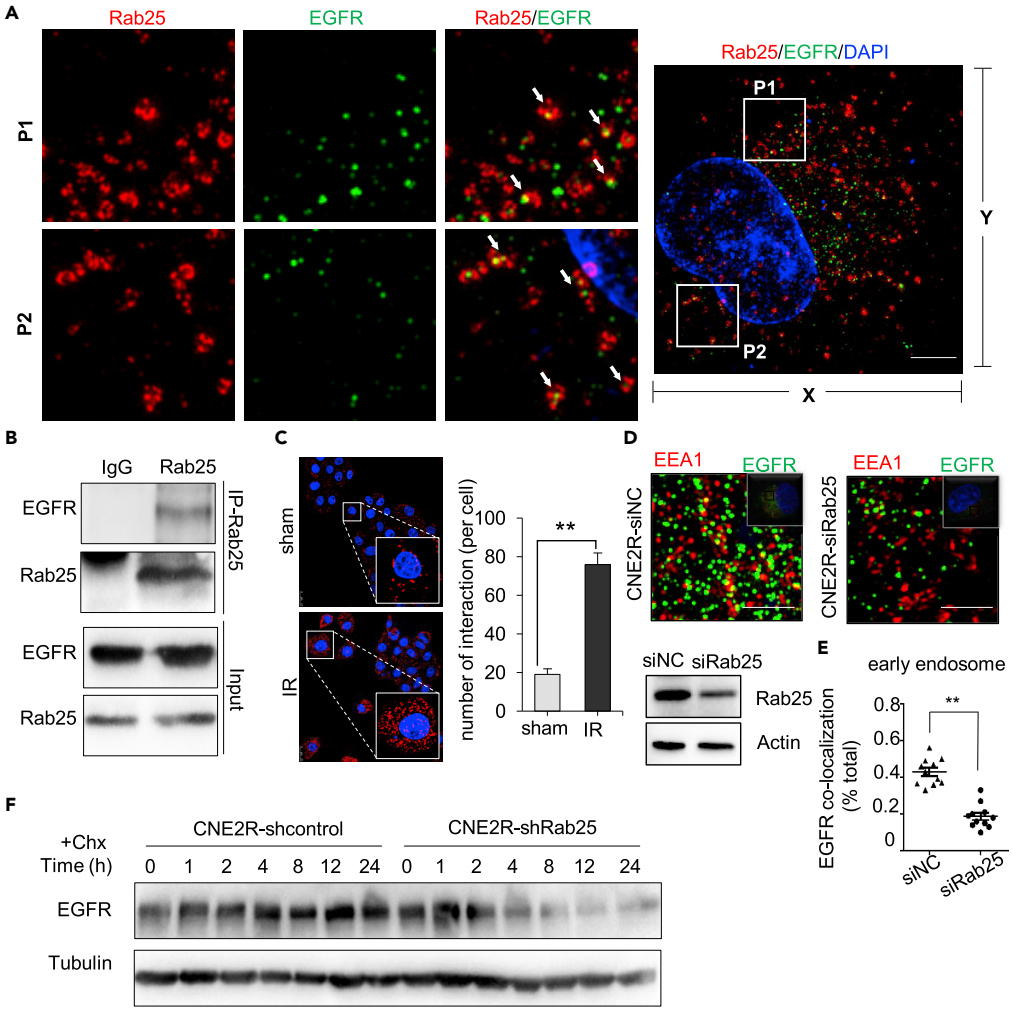

Figure 4. Rab25 Binds and Prevents EGFR Degradation

(A) Images of confocal microscopy of A549R cells stained with antibodies of Rab25 and EGFR and DAPI. White arrows indicate the merged signals. Scale bar of right picture is 2.5 μm.

(B) Rab25 was immunoprecipitated from CNE2R cells, followed by immunoblotting of EGFR and Rab25.

(C) CNE2R cells treated with sham or 5 Gy radiation for 24 h were stained with EGFR and Rab25 antibodies and subjected to Duolink *in situ* PLA. Scale bar, 25 μm. Bar diagrams, the number of interactions per cell. Mean ± SD, **p < 0.01.

(D) Images of confocal microscopy of cells stained with antibodies of EEA1 and EGFR.

(E) Co-localization of EGFR and early endosome marker EEA1. Mean ± SD, **p<0.01.

(F) Immunoblotting of EGFR in CNE2R cells transfected with control or shRab25 and treated with either vehicle (0.01% dimethyl sulfoxide) or 10uM cycloheximide (Chx) for the indicated time.

content of EGFR was decreased when we knockdown Rab25 in CNE2R or A549R cell (Figure 5F), which was supported in other therapeutic-resistant cell lines, including radioresistant H358R and H157R LUAD cells and Taxol-resistant ovarian carcinoma SKOV3R cells (Figures S4B–S4E).

We then examined whether the transportation route of internalized EGFR was influenced by Rab25. A "pulse-chase" experiment Kondapalli et al., 2015 was performed to determine the rate of recycling of internalized EGFR. Cells were incubated with a fixed concentration of EGF (1 ng/mL) for 10 or 30 min (stimulation), washed with acid to remove surface EGF, and subsequently transferred the cells back to 37°C for 10–40 min (rest). At the end of the chase, the amount of cell surface EGFR was quantified by FACS analysis. The results showed that during the "chasing phase" the surface content of EGFR in radioresistant H358R cells was quickly recovered to the original level after 10 min, whereas the content of EGFR in parental cells was only less than 60% of the original level (Figure 5G). In Rab25-overexpressing and control NPC cells, both

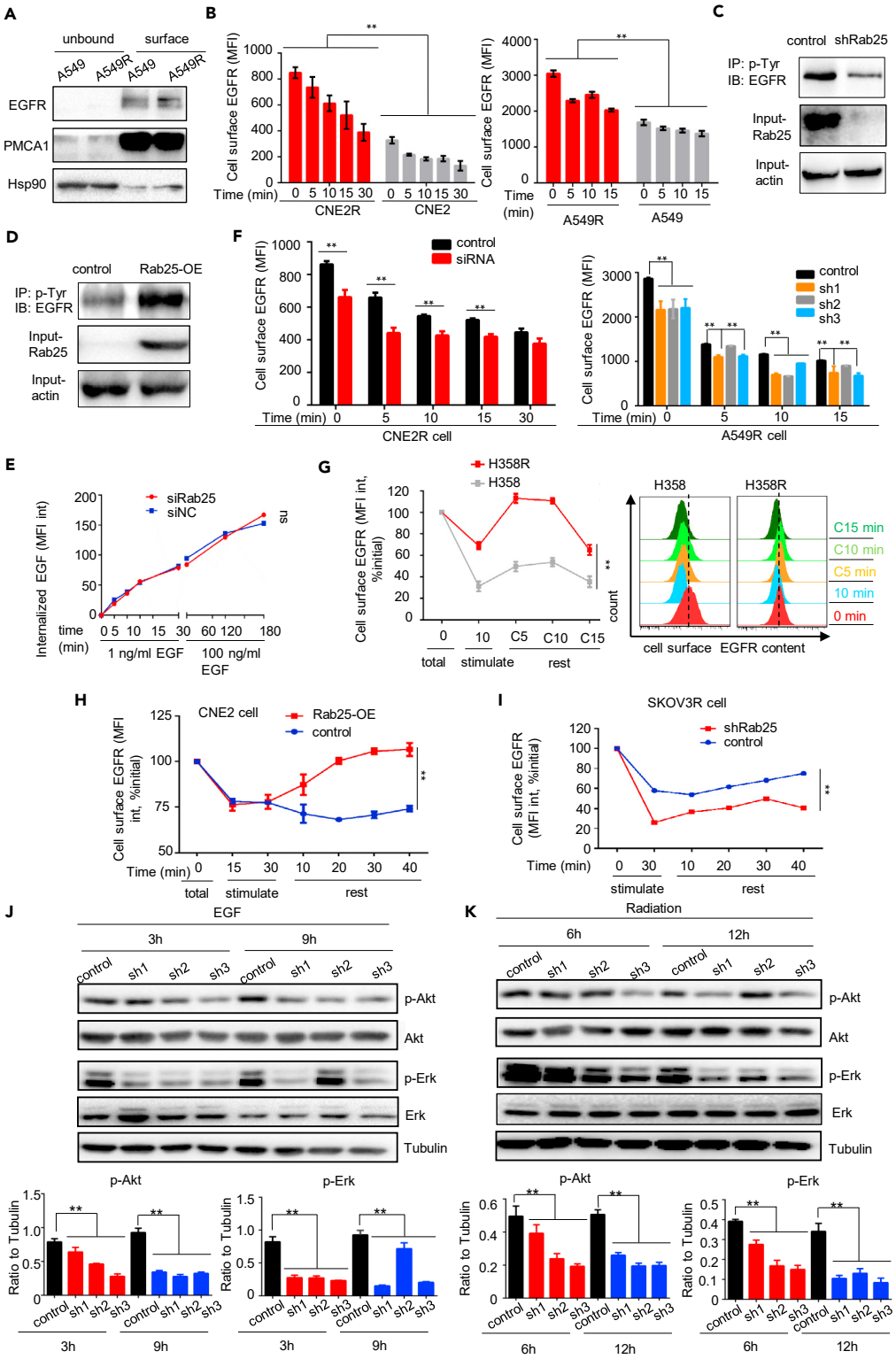

Figure 5. Rab25 Enhances EGFR Recycle and Increases Cell Surface Content of EGFR

(A) Immunoblotting of EGFR on cell surface in A549 and A549R cells. PMCA1 was used as plasma membrane loading control, and Hsp90 was used as cytosol protein control.

Figure 5. *Continued*

(B–D) (B) The kinetics of ligand-induced internalization of EGFR in radioresistant CNE2R cell or A549R cell. Phosphorylated tyrosine (p-Tyr) was immunoprecipitated from CNE2R cells with knockdown (C) or overexpression (D) of Rab25, followed with immunoblotting of EGFR.

(E) Endocytotic rate of EGF in CNE2R cell or CNE2R cells with down-expression of Rab25. The amount of alex-488 conjugated EGF was quantified by flow cytometry.

(F) Quantification of the cell surface content of EGFR in cells or in cells with down-expression of Rab25. EGFR cell surface content was performed every 5 min after stimulation with 1 ng/mL EGF. Right, flow cytometry analysis at each time point was plotted as histogram.

(G) Left, cell surface EGFR recycling rate in H358 or H358R cells pretreated with 1 ng/mL EGF for 10 min before which cells had been starved for 6 h. Right: flow cytometry analysis at each time point was plotted as histogram.

(H and I) (H) Cell surface EGFR recycling rate in CNE2 and CNE2 cells stably transfected with Rab25 or in ovarian carcinoma taxol-resistant SKOV3R cells with knockdown of Rab25 (I). Mean ± SD, $^{**}p < 0.01$.

(J) EGF-induced activation of RTK-mediated signaling pathways in A549R cells and A549R with siRNA-mediated knockdown of Rab25. Cells were first incubated for 6 h in serum-free medium and then treated with 1 ng/mL EGF for indicated time.

(K) Immunoblotting of radiation-induced activation of RTK pathways in A549R cells or in A549R with siRNA-mediated knockdown of Rab25. Cells were irradiated at 4 Gy.

cells had decreased by 25% of the initial value after EGF stimulation for 30 min. During the chasing phase, a small fraction of EGFR molecules was recycled to the cell surface in control cells, and the EGFR membrane content remained at a low level. In contrast, after 40 min of chasing, the membrane content of EGFR nearly reverted to the initial level in Rab25-overexpressing cells (Figure 5H). In addition, suppression of Rab25 in SKOV3R cells severely impaired the trafficking of EGFR onto the cell surface (Figure 5I). We next examined whether hyperactive EGFR signaling in radioresistant cells was dependent on Rab25 expression. After knockdown Rab25 by lenti-viral transduction of Rab25-specific shRNA in radioresistant cells, we found that the phosphorylation of EGFR and activation of Akt and Erk declined when the cells were treated with ligand or radiation (Figures 5J, 5K, and S4F–S4H) and re-expression of Rab25 in Rab25 knockdown cells compensated the declination, suggesting that Rab25 actively participates in regulating RTK protein levels and activity in response to irradiation or ligands. Taken together, these results indicate that Rab25-endosomes are responsible for the enhanced level and activity of EGFR in therapeutic-resistant cancer cells.

Blocking Rab25 Sensitizes Radioresistant Cells with Reversed EMT

The high expression of Rab25 in radioresistant cells indicated its close association with radioresistance. FACS analysis showed an increase in the extent of apoptosis in Rab25-knockdown cells at 24 and 36 h (Figure 6A) after cells received a 4-Gy dose radiation. Colony formation assay further demonstrated that Rab25 depletion markedly suppressed the clonogenicity of CNE2R cells and A549R cells after radiation treatment, especially when the cells received a 6- or 8-Gy dose (Figures 6B and S5A). We also examined the effect of Rab25 knockdown on radiosensitivity of radioresistant H358R cells and chemo-sensitivity of taxol-resistant CNE1-TR cells and observed that both cells became sensitive to therapeutic treatment upon Rab25 knockdown (Figures S5B and S5C). Thus, these results revealed that Rab25 expression contributed to therapeutic resistance of cancer cells. In addition, we also employed a TKI erlotinib to treat PC9 cell to study whether EGFR inhibition could sensitize cancer cells to irradiation. After erlotinib treatment, FACS analysis showed that cells became sensitive to radiation, suggesting that TKIs treatment might increase cell radiosensitivity (Figure S5D).

Most cancer cells exhibit an EMT-like transition when they acquire resistance to therapies. The loss of epithelial features and acquisition of mesenchymal characteristics enable resistant cells to spread more quickly and be more invasive. We observed that, after knocking down of Rab25, the expression of EMT markers in radioresistant CNE2R cells could be reversed (Figure S5E) and cells were sensitive to induction of apoptosis and anoikis (Figures 6C, S5F, and S5G) with inhibited invasiveness (Figure 6D). These observations were further confirmed in taxol-resistant CNE1-TR cells and radioresistant H358R cells transfected with Rab25-specific siRNAs, which showed increased cell apoptosis rates induced by ultra-low attachment treatment. In addition, the sphere formation ability of CNE2R cells was dramatically decreased after Rab25 knockdown (Figure 6E).

Blocking Rab25 Resensitizes Radioresistant Tumors

We wonder whether Rab25 is a therapeutic target to breakdown tumor radioresistance. Using *in vivo* xenograft tumors of CNE2R-shcontrol or CNE2R-shRab25 cells, we found that silencing of Rab25 gene

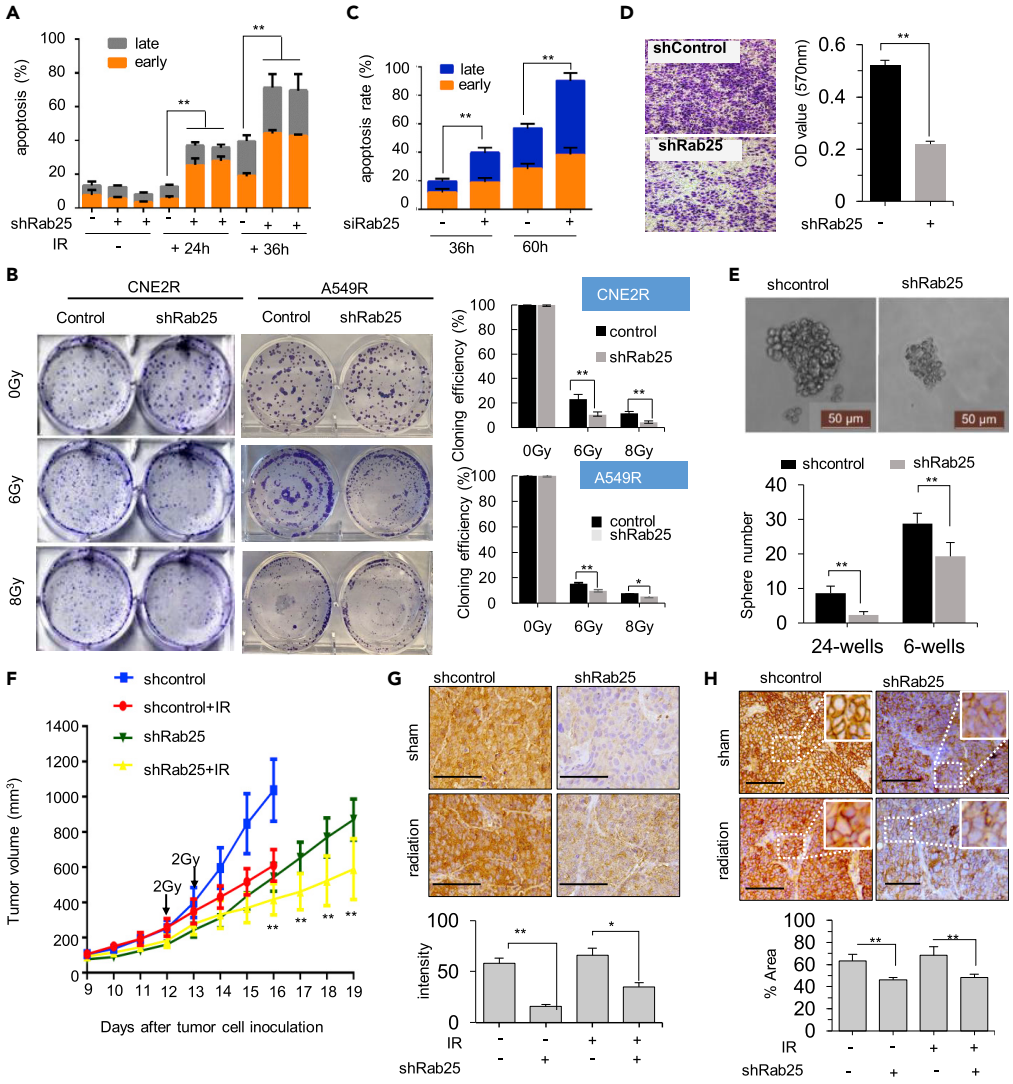

Figure 6. Blocking Rab25 Enhances Cell Death and Radio-Sensitization *In Vitro* and *In Vivo*

(A) Apoptosis rate in CNE2R or CNE2R cells transfected with shRab25 24 or 36 h after 4 Gy radiation.

(B) Clonogenic survival of radiation in radioresistant cells with shRab25-mediated knockdown. The clonogenicity was calculated by normalizing to the control cells that received 0 Gy IR, and the normalized clonogenic survival rates are shown on the bottom (n = 3, mean ± SD, *p < 0. 05, **p < 0. 01).

(C) Apoptosis rate after cells cultured in ultra-low attached wells for indicated time.

(D) Images and capacity of trans-well invasion (au, arbitrary units; n = 3; mean ± SD, **p < 0.01).

(E) Mammosphere formation assay (n = 3 in each group, mean ± SD, **p < 0.01), scale bar, 50 μm.

(F) Radiosensitivity of xenograft tumors generated with control and CNE2R-shRab25 cells and treated with 2 Gy at day 12 and day 13 (n = 5; mean ± SD, **p < 0.01).

(G) Representative images of IHC staining for Rab25 in NPC xenografts with or without irradiation. The average Rab25-positive cells in tumors were quantified and shown in the right bar graph. Scale bar, 50 μm. Mean ± SD, *p < 0.05, **p < 0.01.

(H) Representative images of IHC staining for EGFR in NPC xenografts with or without irradiation. The average EGFR-positive cells in tumors were quantified and shown in the right bar graph. Scale bar, 50 μm. mean ± SD, **p < 0.01.

expression significantly suppress tumor growth (Figure 6F, blue line versus green line). From day 16, the radiation-treated group of shRab25 xenografts showed an obvious reduction in tumor growth rate compared with other three groups (Figure 6F). The knockdown efficiency of Rab25 in these xenografts was confirmed using IHC staining (Figure 6G), and down-expression of EGFR (Figure 6H) was observed

in xenografts knockdown Rab25. These results demonstrate that Rab25-mediated EGFR enhancement is critically required for tumor cells to survive radiation.

DISCUSSION

This study reveals a potential therapeutic target of Rab25-mediated EGFR enhancement in radioresistant LUAD and NPC cells. Rad25 has been linked with a poor prognosis in several cancer types (Cheng et al., 2004; Zhang et al., 2013a), and our current results further demonstrate a function of Rab25 in recycling EGFR, which is responsible for the acquired radioresistance in LUAD and NPC cells. Rab25 interacts with EGFR to reduce the degradation of EGFR leading to the enhancement of EGFR richness on cell surface causing an increased RTK-mediated signaling and aggressive phenotype of the radioresistant cancer cells. These findings suggest a model of Rab25-mediated EGFR recycling in acquired radioresistance, in which the formation of Rab25-EGFR conjugates in the cytoplasm is able to reduce the degradation of eternized EGFR and to recycle them to the cell surface required for the surviving tumor cells to keep the essential proliferation capacity and regrow under genotoxic stress conditions such as radiotherapy.

Although long being discovered, few studies has revealed the exact function of Rab25. The association between Rab25 and wild-type EGFR was first observed in lung cancer, where Rab25 inhibition promoted the endocytosis of EGFR and thus contributed to gefitinib sensitization (Jo et al., 2014). Jeong et al. recently reported that Rab25-induced tumor EMT was regulated by integrin/EGFR/VEGF-A/Snail axis, suggesting Rab25-EGFR interaction plays an important role in tumor migration (Jeong et al., 2018). In this paper, we first and directly proved that Rab25 regulated EGFR content and activation by fast recycling EGFR to cell surface upon ligand or stress stimulation, adding a significant information on tumor adaptive response to therapeutic radiation. Not only EGFR content but also phosphorylation status of EGFR was influenced by Rab25 expression. EGFR recruitment into endosomes was dependent on Grb2 (Johannessen et al., 2006; Jiang et al., 2003), which in this study was observed to co-localize with Rab25. In addition, GAB1, a scaffold protein in amplification of EGFR-mediated PI3K activation (Mattoon et al., 2004), was found in Rab25-EGFR co-localized complex, suggesting that EGFR located in Rab25-endosome was active in signaling transduction.

Rab25-mediated EGFR recycling will also provide mechanistic insights in revealing tumor acquired resistance to TKIs. EGFR TKIs alone or in combination with other treatment strategies are now the recommended treatment for patients with lung cancer harboring mutant EGFR. However, patients with mutant EGFR eventually develop acquired TKI resistance and patients harboring wild-type EGFR show poor response to first-generation TKIs and serious side effect for second- or third-generation TKIs (Liao et al., 2015). Moreover, EGFR mutation in non-small-cell lung cancer of adenocarcinoma histology ranges from roughly 12%–47% (Midha et al., 2015), implying that there are a lot of patients with lung cancer with wild-type EGFR who cannot benefit from TKIs treatment. Our finding that wild-type EGFR was tightly controlled by Rab25 provided a possibility to develop generation of TKIs, especially after identification of Rab25-EGFR interaction motif. In addition, we observed that other RTK-like receptors including Met, RYK, EphB2, and EphB6 were also regulated by Rab25, suggesting that Rab25-endosome might be one of the main RTK trafficking route in radioresistant cells. Considering the cross talk between different RTK members, we believed Rab25 might be a promising target for inhibiting RTK-mediated signaling pathway.

In this study, we illustrated that Rab25 was acquired for radioresistance in two major solid tumors treated by radiotherapy, which was linked with EMT enhancement and survival advantage under anchorage-independent environment. The EMT plasticity of a cancer cell is a major feature of therapy-resistant tumors. The adaptive tumor resistance and increased metastasis constitute the major failure of anti-cancer therapy causing 90% of cancer mortalities (Ahmed et al., 2018) in which acquired EMT-like phenotype and enhanced survival ability are linked with RTK-mediated pathway (Buchheit et al., 2014). RTK-mediated signaling pathways are often hyperactive in EMT program, which were activated by growth factors and then rendered the tight junction of cells (Forster, 2008; Ray and Jablons, 2009). The EGFR content on the cell surface is functionally important for activating EGFR downstream signaling. Here, we observed a rapid recovery of the EGFR surface level in Rab25 over-expressing cells. High expression of Rab25 greatly promotes its binding to EGFR and accelerated the recovery of EGFR content on cell membrane. Downregulation of Rab25 led to a reversal of EMT-like markers and reduced anti-anoikis ability, indicating that EMT occurrence in therapeutic-resistant cells is partially Rab25 dependent. Our current results provide new insights into the mechanisms of how therapeutic-resistant cells acquire EMT plasticity, suggesting that Rab25 is a potential effective target to block EGFR signaling and tumor proliferation.

By analyzing samples from 101 patients with NPC, we demonstrate that the expression of Rab25 in NPC was highly related to the radiotherapy response. However, the level of Rab25 expression did not seem to be associated with the histological grade, tumor size, or regional nodal metastasis. In patients with lung cancer, the same is true that high expression of Rab25 renders a poorer survival rate. The majority of patients with lung cancer are clinically diagnosed at advanced stages with a poor survival rate (Zappa and MOUSA, 2016). Particularly, these patients who lack surgical indications are recommended to receive radiotherapy (Postmus et al., 2017). For NPC, owing to its anatomical features and relative sensitivity to radiation, radiotherapy has been a first-line treatment (Zhang et al., 2013b). Although radiotherapy can control local tumor, radioresistance always occurs and becomes a challenging obstacle for curative lung cancer and NPC treatment. This highlights the Rab25-dependent effect on radiotherapy efficacy in patients with cancer.

Given the importance of Rab25 and the EGFR signaling pathway in human cancers in general, Rab25 may also represent a predictive marker for the cancer radiotherapy response and a potential candidate target for enhancing therapeutic efficacy. Further elucidating the molecular mechanisms underlying Rab25 controlled activation and duration of EGFR signaling may invent additional targets for desensitization of resistant tumor cells.

Limitation of the Study

In this study, we found that hyperactivation of RTK-mediated signaling pathways in therapeutic-resistant cells was due to rapid recycling of EGFR mediated by Rab25. Although a positive correlation between Rab25 expression and other RTKs such as MET and IGF1R was also observed, the detailed clarification was not performed, which warrants further investigation.

METHODS

All methods can be found in the accompanying Transparent Methods supplemental file.

SUPPLEMENTAL INFORMATION

Supplemental Information can be found online at https://doi.org/10.1016/j.isci.2020.100997.

ACKNOWLEDGMENTS

We acknowledge Dr. David Gandara and Dr. Megan Daily at University of California Davis for discussion on clinic lung cancer treatment and the TCGA database for providing the data and analyses in this article. This study was partially supported by the grants from National Natural Science Foundation of China, 81602679 (to L.Z.), 81530084 (to L.-Q.S.) and 81672509 (to B.X.), and 81602406 (to Z.L.), 81874200, 81572750, and US National Cancer Institute Grants (CA152313 to J.J.L.). The costs of publication of this article were defrayed in part by the payment of page charges. This article must therefore be hereby marked advertisement in accordance with 18 U. S. C. Section 1734 solely to indicate this fact.

AUTHOR CONTRIBUTIONS

Conception and design: L.-Q.S., L.Z., J.J.L. Development of methodology: L.Z., M.F. Acquisition of data (provided animals, acquired and managed patients, provided facilities, etc.): L.Z., B.X., Y.Q., J.Z., Z.L. Analysis and interpretation of data (e.g., statistical analysis, biostatistics, computational analysis): L.Z., L.-Q.S., J.J.L., B.X. Writing, review, and/or revision of the manuscript: L.Z., L.-Q.S., J.J.L., B.X. Administrative, technical, or material support (i.e., reporting or organizing data, constructing databases): M.F., Y.D., D.J., Y.Q., R.T., J.H.

DECLARATION OF INTERESTS

No potential conflicts of interest were disclosed.

Received: October 23, 2019
Revised: February 18, 2020
Accepted: March 17, 2020
Published: April 24, 2020

REFERENCES

Ahmed, K.A., Scott, J.G., Arrington, J.A., Naghavi, A.O., Grass, G.D., Perez, B.A., Caudell, J.J., Berglund, A.E., Welsh, E.A., Eschrich, S.A., et al. (2018). Radiosensitivity of lung metastases by primary histology and implications for stereotactic body radiation therapy using the genomically adjusted radiation dose. J. Thorac. Oncol. *13*, 1121–1127.

Aravindan, N., Aravindan, S., Pandian, V., Khan, F.H., Ramraj, S.K., Natt, P., and Natarajan, M. (2014). Acquired tumor cell radiation resistance at the treatment site is mediated through radiation-orchestrated intercellular communication. Int. J. Radiat. Oncol. Biol. Phys. *88*, 677–685.

Begg, A.C., Stewart, F.A., and Vens, C. (2011). Strategies to improve radiotherapy with targeted drugs. Nat. Rev. Cancer *11*, 239–253.

Buchheit, C.L., Weigel, K.J., and Schafer, Z.T. (2014). Cancer cell survival during detachment from the ECM: multiple barriers to tumour progression. Nat. Rev. Cancer *14*, 632–641.

Camidge, D.R., Pao, W., and Sequist, L.V. (2014). Acquired resistance to TKIs in solid tumours: learning from lung cancer. Nat. Rev. Clin. Oncol. *11*, 473–481.

Casaletto, J.B., and Mcclatchey, A.I. (2012). Spatial regulation of receptor tyrosine kinases in development and cancer. Nat. Rev. Cancer *12*, 387–400.

Casanova, J.E., Wang, X., Kumar, R., Bhartur, S.G., Navarre, J., Woodrum, J.E., Altschuler, Y., Ray, G.S., and Goldenring, J.R. (1999). Association of Rab25 and Rab11a with the apical recycling system of polarized Madin-Darby canine kidney cells. Mol. Biol. Cell *10*, 47–61.

Caswell, P.T., Spence, H.J., Parsons, M., White, D.P., Clark, K., Cheng, K.W., Mills, G.B., Humphries, M.J., Messent, A.J., Anderson, K.I., et al. (2007). Rab25 associates with alpha5beta1 integrin to promote invasive migration in 3D microenvironments. Dev. Cell *13*, 496–510.

Ceresa, B.P. (2012). Spatial regulation of epidermal growth factor receptor signaling by endocytosis. Int. J. Mol. Sci. *14*, 72–87.

Cheng, K.W., Agarwal, R., Mitra, S., Lee, J.S., Carey, M., Gray, J.W., and Mills, G.B. (2012). Rab25 increases cellular ATP and glycogen stores protecting cancer cells from bioenergetic stress. EMBO Mol. Med. *4*, 125–141.

Cheng, K.W., Lahad, J.P., Kuo, W.L., Lapuk, A., Yamada, K., Auersperg, N., Liu, J., Smith-Mccune, K., Lu, K.H., Fishman, D., et al. (2004). The RAB25 small GTPase determines aggressiveness of ovarian and breast cancers. Nat. Med. *10*, 1251–1256.

Chung, J.H., Rho, J.K., Xu, X., Lee, J.S., Yoon, H.I., Lee, C.T., Choi, Y.J., Kim, H.R., Kim, C.H., and Lee, J.C. (2011). Clinical and molecular evidences of epithelial to mesenchymal transition in acquired resistance to EGFR-TKIs. Lung Cancer *73*, 176–182.

Dozynkiewicz, M.A., Jamieson, N.B., Macpherson, I., Grindlay, J., van den Berghe, P.V., von Thun, A., Morton, J.P., Gourley, C., Timpson, P., Nixon, C., et al. (2012). Rab25 and CLIC3 collaborate to promote integrin recycling from late endosomes/lysosomes and drive cancer progression. Dev. Cell *22*, 131–145.

Forster, C. (2008). Tight junctions and the modulation of barrier function in disease. Histochem. Cell Biol. *130*, 55–70.

Fu, S., Li, Z., Xiao, L., Hu, W., Zhang, L., Xie, B., Zhou, Q., He, J., Qiu, Y., Wen, M., et al. (2019). Glutamine synthetase promotes radiation resistance via facilitating nucleotide metabolism and subsequent DNA damage repair. Cell Rep. *28*, 1136–1143 e4.

Guo, G., Yan-Sanders, Y., Lyn-Cook, B.D., Wang, T., Tamae, D., Ogi, J., Khaletskiy, A., Li, Z., Weydert, C., Longmate, J.A., et al. (2003). Manganese superoxide dismutase-mediated gene expression in radiation-induced adaptive responses. Mol. Cell Biol. *23*, 2362–2378.

Hasselbach, L., Haase, S., Fischer, D., Kolberg, H.C., and Sturzbecher, H.W. (2005). Characterisation of the promoter region of the human DNA-repair gene Rad51. Eur. J. Gynaecol Oncol. *26*, 589–598.

Hehnly, H., and Doxsey, S. (2014). Rab11 endosomes contribute to mitotic spindle organization and orientation. Dev. Cell *28*, 497–507.

Higgins, G.S., Krause, M., Mckenna, W.G., and Baumann, M. (2016). Personalized radiation oncology: epidermal growth factor receptor and other receptor tyrosine kinase inhibitors. Recent Results Cancer Res. *198*, 107–122.

Hou, Y., Zhu, Q., Li, Z., Peng, Y., Yu, X., Yuan, B., Liu, Y., Yin, L., Jiang, Z., Li, J., et al. (2017). The FOXM1-ABCC5 axis contributes to paclitaxel resistance in nasopharyngeal carcinoma cells. Cell Death Dis. *8*, e2659.

Huang, S., Ll, C., Armstrong, E.A., Peet, C.R., Saker, J., Amler, L.C., Sliwkowski, M.X., and Harari, P.M. (2013). Dual targeting of EGFR and HER3 with MEHD7945A overcomes acquired resistance to EGFR inhibitors and radiation. Cancer Res. *73*, 824–833.

Jakobsen, K.R., Demuth, C., Sorensen, B.S., and Nielsen, A.L. (2016). The role of epithelial to mesenchymal transition in resistance to epidermal growth factor receptor tyrosine kinase inhibitors in non-small cell lung cancer. Transl Lung Cancer Res. *5*, 172–182.

Jeong, B.Y., Cho, K.H., Jeong, K.J., Park, Y.Y., Kim, J.M., Rha, S.Y., Park, C.G., Mills, G.B., Cheong, J.H., and Lee, H.Y. (2018). Rab25 augments cancer cell invasiveness through a beta1 integrin/EGFR/VEGF-A/Snail signaling axis and expression of fascin. Exp. Mol. Med. *50*, e435.

Jiang, X., Huang, F., Marusyk, A., and Sorkin, A. (2003). Grb2 regulates internalization of EGF receptors through clathrin-coated pits. Mol. Biol. Cell *14*, 858–870.

Jo, U., Park, K.H., Whang, Y.M., Sung, J.S., Won, N.H., Park, J.K., and Kim, Y.H. (2014). EGFR endocytosis is a novel therapeutic target in lung cancer with wild-type EGFR. Oncotarget *5*, 1265–1278.

Johannessen, L.E., Pedersen, N.M., Pedersen, K.W., Madshus, I.H., and Stang, E. (2006). Activation of the epidermal growth factor (EGF) receptor induces formation of EGF receptor- and Grb2-containing clathrin-coated pits. Mol. Cell Biol *26*, 389–401.

Kondapalli, K.C., Llongueras, J.P., Capilla-Gonzalez, V., Prasad, H., Hack, A., Smith, C., Guerrero-Cazares, H., Quinones-Hinojosa, A., and Rao, R. (2015). A leak pathway for luminal protons in endosomes drives oncogenic signalling in glioblastoma. Nat. Commun. *6*, 6289.

Li, G., Liu, Y., Su, Z., Ren, S., Zhu, G., Tian, Y., and Qiu, Y. (2013). MicroRNA-324-3p regulates nasopharyngeal carcinoma radioresistance by directly targeting WNT2B. Eur. J. Cancer *49*, 2596–2607.

Liao, B.C., Lin, C.C., and Yang, J.C. (2015). Second and third-generation epidermal growth factor receptor tyrosine kinase inhibitors in advanced nonsmall cell lung cancer. Curr. Opin. Oncol. *27*, 94–101.

Maranto, C., Udhane, V., Hoang, D.T., Gu, L., Alexeev, V., Malas, K., Cardenas, K., Brody, J.R., Rodeck, U., and Bergom, C. (2018). STAT5A/B Blockade Sensitizes Prostate Cancer to Radiation through Inhibition of RAD51 and DNA Repair. Clin. Cancer Res. *24*, 1917–1931.

Mattoon, D.R., Lamothe, B., Lax, I., and Schlessinger, J. (2004). The docking protein Gab1 is the primary mediator of EGF-stimulated activation of the PI-3K/Akt cell survival pathway. BMC Biol. *2*, 24.

Midha, A., Dearden, S., and Mccormack, R. (2015). EGFR mutation incidence in non-small-cell lung cancer of adenocarcinoma histology: a systematic review and global map by ethnicity (mutMapII). Am. J. Cancer Res. *5*, 2892–2911.

Mitra, S., Montgomery, J.E., Kolar, M.J., Li, G., Jeong, K.J., Peng, B., Verdine, G.L., Mills, G.B., and Moellering, R.E. (2017). Stapled peptide inhibitors of RAB25 target context-specific phenotypes in cancer. Nat. Commun. *8*, 660.

Postmus, P.E., Kerr, K.M., Oudkerk, M., Senan, S., Waller, D.A., Vansteenkiste, J., Escriu, C., and Peters, S. (2017). Early and locally advanced non-small-cell lung cancer (NSCLC): ESMO Clinical Practice Guidelines for diagnosis, treatment and follow-up. Ann. Oncol. *28*, iv1–iv21.

Ray, M., and Jablons, D. (2009). Lung cancer metastasis novel biological mechanisms and impact on clinical practice. Hallmarks of Metastasis, 29–46.

Ricordel, C., Friboulet, L., Facchinetti, F., and Soria, J.C. (2018). Molecular mechanisms of acquired resistance to third-generation EGFR-TKIs in EGFR T790M-mutant lung cancer. Ann. Oncol. *29*, i28–i37.

Shapira, I., Lee, A., Vora, R., and Budman, D.R. (2013). P53 mutations in triple negative breast cancer upregulate endosomal recycling of epidermal growth factor receptor (EGFR)

increasing its oncogenic potency. Crit. Rev. Oncol. Hematol. *88*, 284–292.

Tan, X., Lambert, P.F., Rapraeger, A.C., and Anderson, R.A. (2016). Stress-induced EGFR trafficking: mechanisms, functions, and therapeutic implications. Trends Cell Biol *26*, 352–366.

Tomas, A., Vaughan, S.O., burgoyne, T., Sorkin, A., Hartley, J.A., Hochhauser, D., and Futter, C.E. (2015). Wash and Tsg101/ALIX-dependent diversion of stress-internalized EGFR from the canonical endocytic pathway. Nat. Commun. *6*, 7324.

Ye, Q.H., Zhu, W.W., Zhang, J.B., Qin, Y., Lu, M., Lin, G.L., Guo, L., Zhang, B., Lin, Z.H., Roessler, S., et al. (2016). GOLM1 modulates EGFR/RTK cell-surface recycling to drive hepatocellular carcinoma metastasis. Cancer Cell *30*, 444–458.

You, S., Li, R., Park, D., Xie, M., Sica, G.L., Cao, Y., Xiao, Z.Q., and Deng, X. (2014). Disruption of STAT3 by niclosamide reverses radioresistance of human lung cancer. Mol. Cancer Ther. *13*, 606–616.

Zappa, C., and Mousa, S.A. (2016). Non-small cell lung cancer: current treatment and future advances. Transl Lung Cancer Res. *5*, 288–300.

Zhang, J., Wei, J., Lu, J., Tong, Z., Liao, B., Yu, B., Zheng, F., Huang, X., Chen, Z., Fang, Y., et al. (2013a). Overexpression of Rab25 contributes to metastasis of bladder cancer through induction of epithelial-mesenchymal transition and activation of Akt/GSK-3beta/Snail signaling. Carcinogenesis *34*, 2401–2408.

Zhang, L., Chen, Q.Y., Liu, H., Tang, L.Q., and Mai, H.Q. (2013b). Emerging treatment options for nasopharyngeal carcinoma. Drug Des. Devel Ther. *7*, 37–52.

Zhang, X., Li, W., Li, H., Ma, Y., He, G., and Tan, G. (2012). Genomic methylation profiling combined with gene expression microarray reveals the aberrant methylation mechanism involved in nasopharyngeal carcinoma taxol resistance. Anticancer Drugs *23*, 856–864.

Zhou, Z., Zhang, L., Xie, B., Wang, X., Yang, X., Ding, N., Zhang, J., Liu, Q., Tan, G., Feng, D., and Sun, L.Q. (2015). FOXC2 promotes chemoresistance in nasopharyngeal carcinomas via induction of epithelial mesenchymal transition. Cancer Lett. *363*, 137–145.

Zwang, Y., and Yarden, Y. (2006). p38 MAP kinase mediates stress-induced internalization of EGFR: implications for cancer chemotherapy. EMBO J. *25*, 4195–4206.

iScience, Volume *23*

Supplemental Information

Rab25-Mediated EGFR Recycling Causes Tumor Acquired Radioresistance

Lu Zhang, Bowen Xie, Yanfang Qiu, Di Jing, Jing Zhang, Yumei Duan, Zhi Li, Ming Fan, Jiang He, Yuanzheng Qiu, Rong Tan, Jian Jian Li, and Lun-Quan Sun

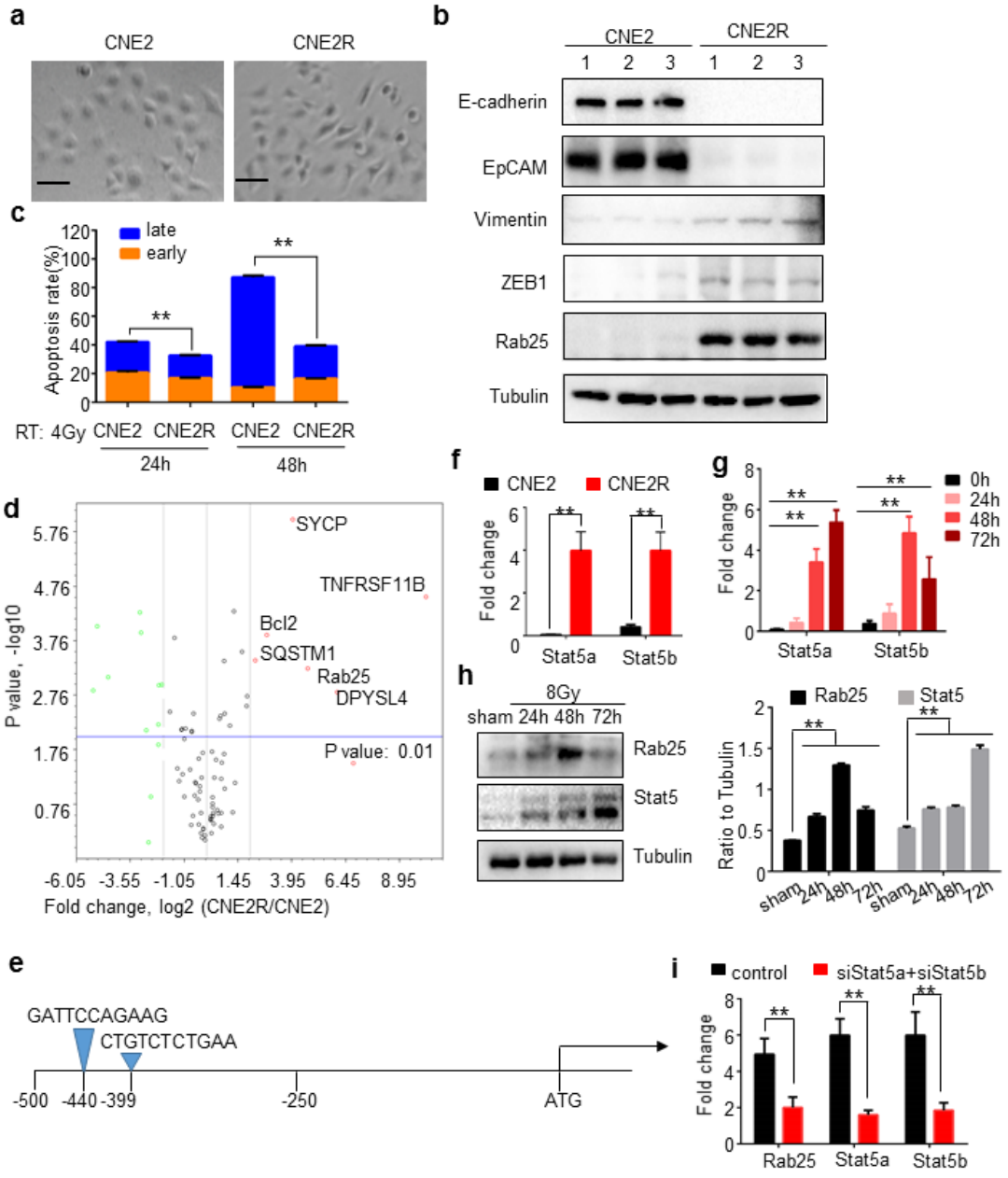

Figure S1 High expression of Rab25 in radioresistant cells was regulated by Stat5, Related to Figure 1.

a Morphological characterization of CNE2 and CNE2R cells (magnification: ×100). **b** Western blotting assay of EMT markers in CNE2 or CNE2R cells. α-Tubulin was used as a loading control. **c** Apoptosis rate of CNE2 or CNE2R cells after culturing in ultra-low attachment wells for indicated time. **d** Volcano plot of differentially genes between CNE2 and CNE2R cells. The total RNAs extracted from CNE2R or CNE2 cells were reverse-transcribed into single-stranded cDNA. Quantitative RT-PCR for cell death-

related genes was performed using the RT² Profiler™ PCR Array Human Cell Death Pathway Finder, and data analysis was performed using a website-based analysis tool from the Qiagene GeneGlobe Data Analysis Center. **e** Diagram to show the predicted binding sites of Stat5 in -500bp region of Rab25. **f** Transcriptional level of Stat5a and Stat5b in CNE2 and CNE2R cells, n=3, mean ± SD, **p < 0.01. **g** Transcriptional level of Stat5a and Stat5b in CNE2 cells irradiated at 8Gy with indicated time. n=3, mean ± SD, **p < 0.01. **h** Protein level of Rab25 or Stat5 in CNE2 cells irradiated at 8Gy with indicated time. **i** Transcriptional level of Rab25, Stat5a, and Stat5b in CNE2R cells or in CNE2R cells with Stat5 knockdown. n=3, mean ± SD, **p < 0.01.

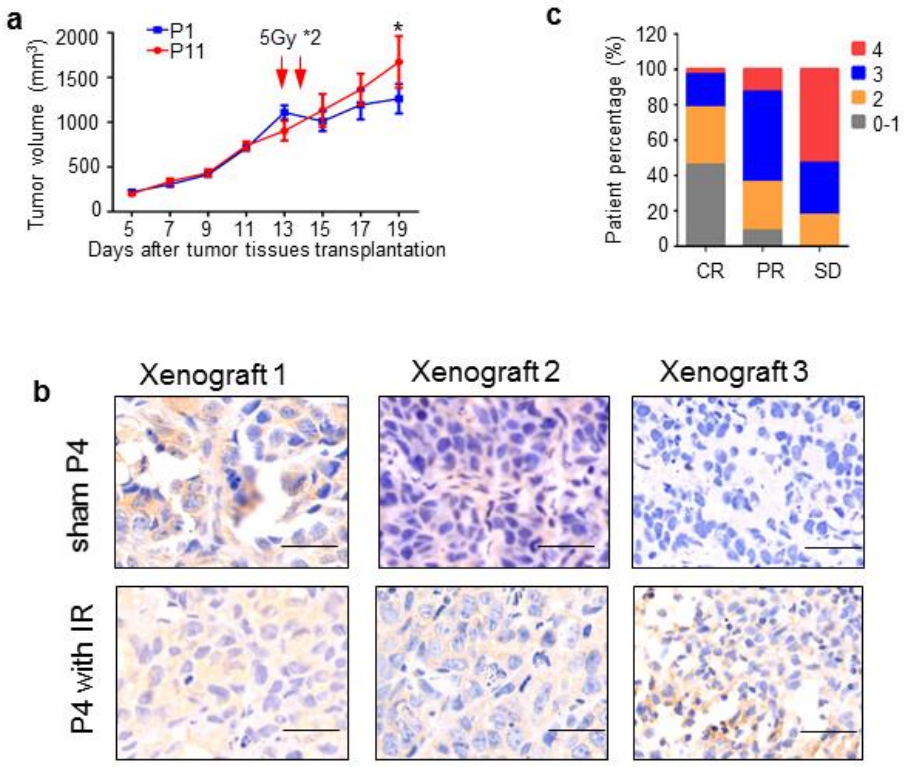

Figure S2 Rab25 was enhanced in radioresistant P4 xenografts, Related to Figure 2.

a Growth curve of tumors from transplanted P1 and P11 mice following radiation. Tumors were irradiated with 5 Gy x 2 when tumor reached 200 mm^3. Four mice were used in each group and data are represented as mean ± SD. The statistical significance between groups was determined with the two-tailed unpaired Student's t test. P values are presented as star marks in figures: *$p < 0.05$. **b** Representative IHC staining of Rab25 in sham P4 (passage alone without radiation) and P4 xenografts. scale bar, 50 μm. **c** Scores of negative, low, medium or high levels of Rab25 were shown as percentage for Rab25 IHC analysis.

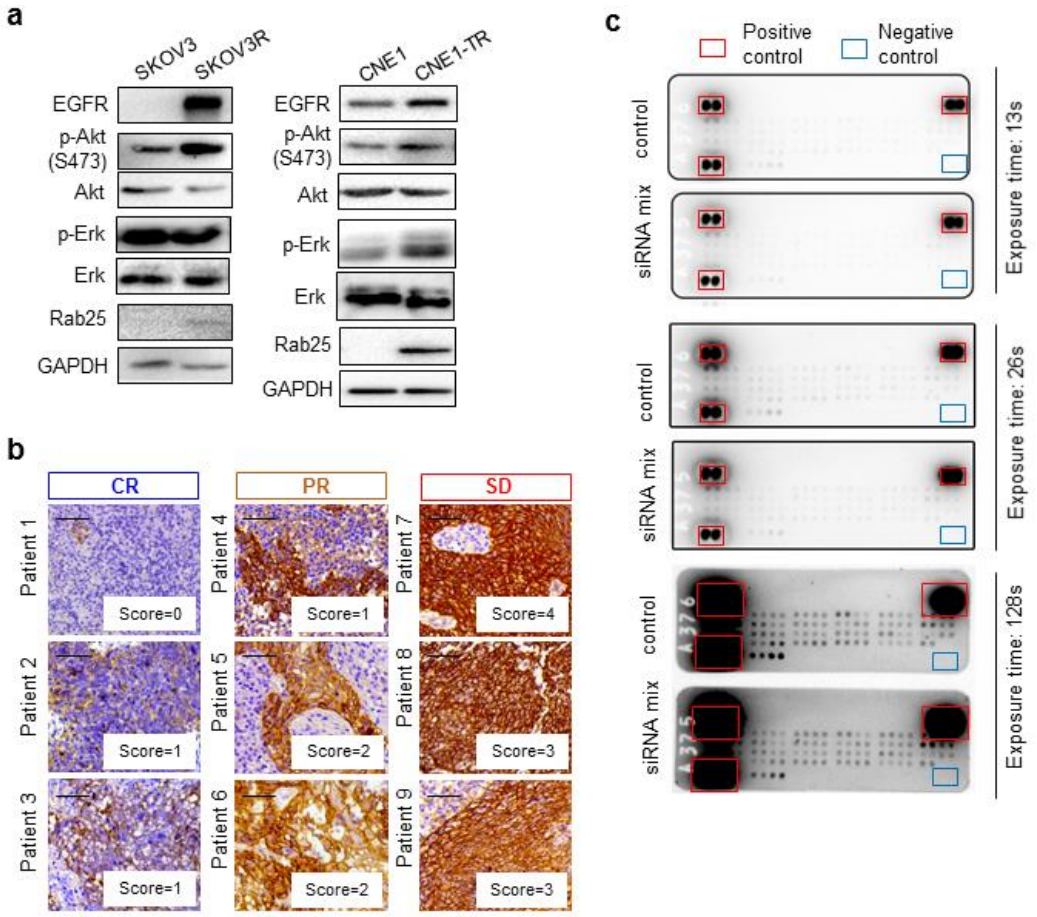

Figure S3 EGFR was hyperactive in therapeutic cells and patients samples, Related to Figure 3.

a Western blot analysis of EGFR and its downstream Erk and Akt signaling pathways in two taxol-resistant cell lines (NPC cell CNE1-TR and ovarian carcinoma cell SKOV3R). **b** Representative IHC staining of EGFR in tissues of NPC patients with different radiotherapy responses. The ASCO-CAP guideline 201336 was used for interpretation of EGFR IHC data. Expression levels of EGFR were classified into five grades (score 0-1: 0-25% , score 2: 25%-50%, score 3: 50%-75%, score 4: >75%). scale bar 50μm. **c** Protein array analysis with different exposure time.

Figure S4

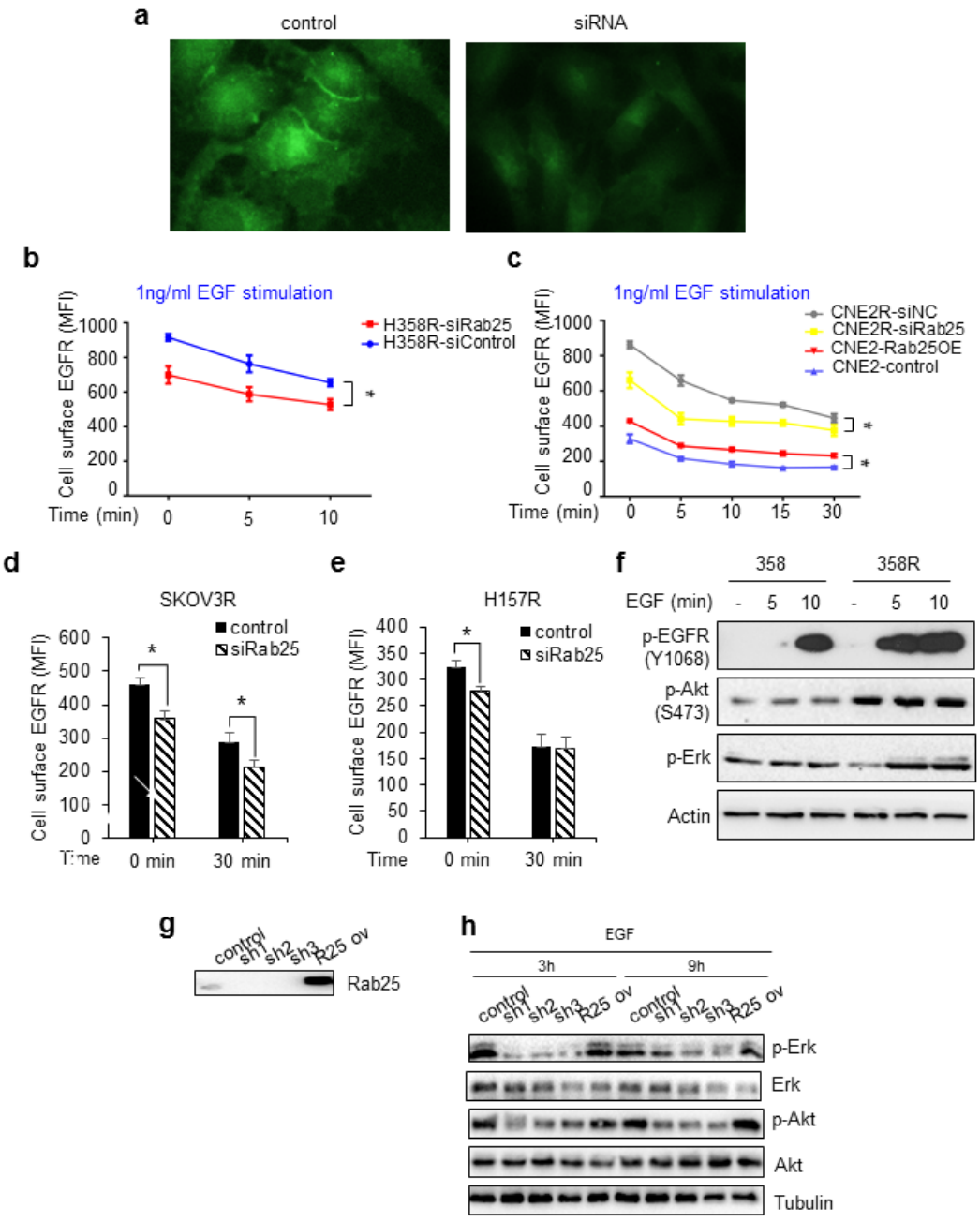

Figure S4 Surface content of EGFR was regulated by Rab25, Related to Figure 5.

a Immonoflourence of EGFR in CNE2R cell or in CNE2R cells with Rab25 knockdown. **b** Quantification of cell surface EGFR content in H358R cells transfected with siControl or siRab25 mix over time following stimulation with 1 ng/ml EGF. **c** EGFR cell surface content by flow cytometry. Each time point for each cell line contained three replicates. Mean ± SD, *p < 0.05. **d,e** Taxol-resistant SKOVR3 or radioresistant

157R cells were firstly transfected with control or siRab25 mixture for 24h. Then, the transfected cells were stimulated with 1 ng/ml EGF for 30 mins. Cells were collected and analyzed for surface EGFR content with Alexa647-conjugated EGFR antibody by FACS. **f** Activity of EGFR downstream signaling Akt and Erk in H358 or H358R cells after short-time EGF stimulation. n=3, mean ± SD, *$p < 0.05$. **g** Rab25 expression in three CNE2R-shRab25 cells and in CNE2R-shRab25 cell transfected with Rab25. **h** Down-expression of Rab25 reduced the expression of EGFR and the activation of associated signaling pathways in radioresistant cells.

Figure S5

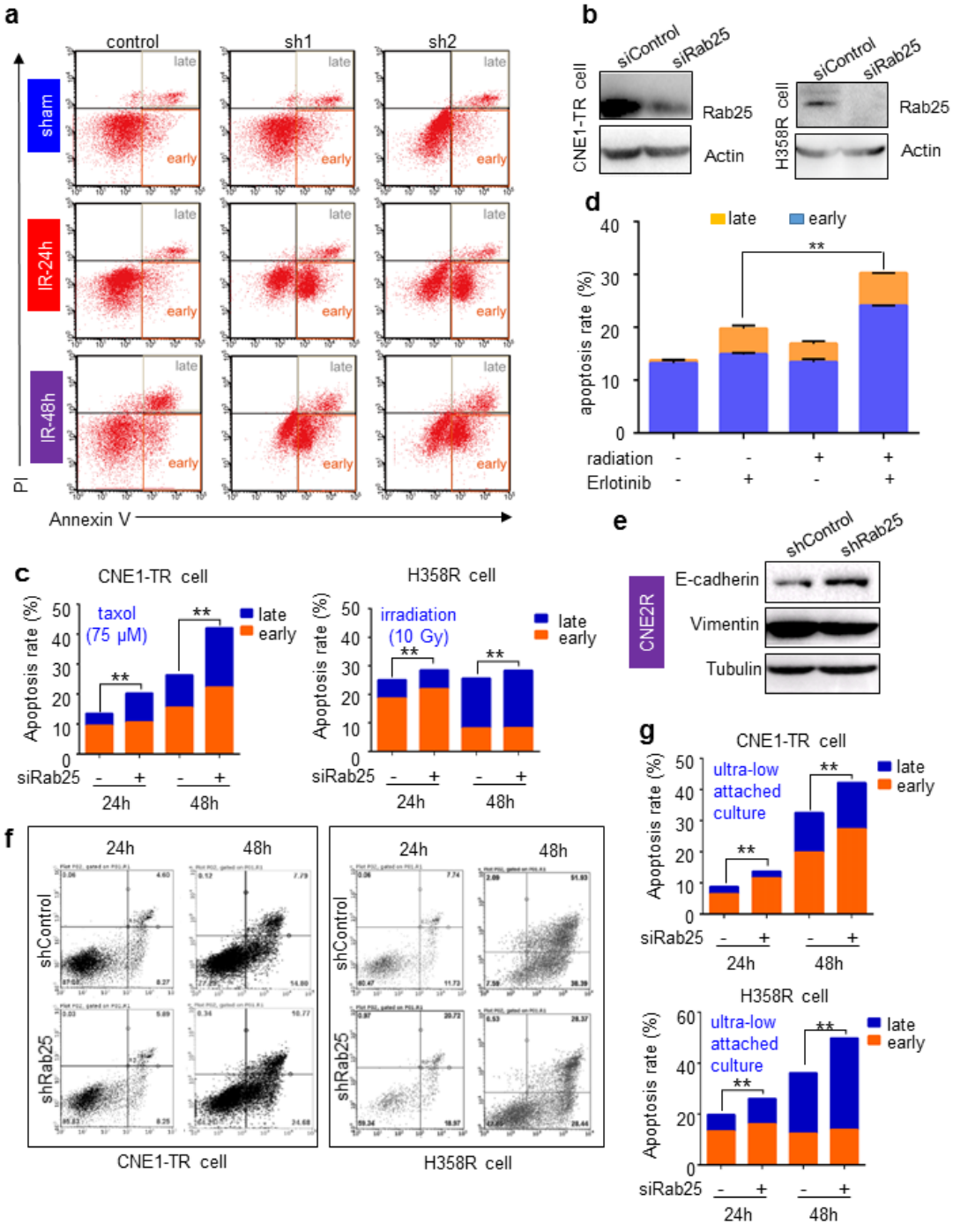

Figure S5 Rab25 knockdown by reverted cell EMT-like phenotype and sensitized cell to radiation, Related to Figure 6.

a Gating strategies for apoptosis induced by radiation in CNE2R cells with or without transfection of shRab25. **b** Rab25 expression in therapeutic-resistant cells was transfected with Rab25 siRNA mixture. **c** Rab25 knockdown increased the apoptosis rate of therapeutic-resistant cells treated with taxol or radiation. The ratio of apoptotic

cells was measured by FACS using Annexin V and PI double staining method. **d** Erlotinib increased the radiation-induced apoptosis of EGFR mutant PC9 cells. Cellls were treated with 5uM Erlotinib alone or combined with 4Gy irradiation. The ratio of apoptotic cells was measured by FACS using Annexin V and PI double staining method. n=3, mean ± SD, **p < 0.01. **e** Decreased expression of EMT-markers in CNE2R cells knockdown with Rab25. **f** Gating strategies for apoptosis induced by detachment in CNE2R cells with or without transfection of shRab25. **g** Rab25 knockdown increased the apoptosis rate of therapeutic-resistant cells cultured in low-attachment culture dishes for the indicated time. n=3, mean ± SD, **p < 0.01.

Table S1. Transcription of Rab25 in different cancers, Related to Figure 2

Variables	n	Rab25 expression			p-value*
		negative/low	moderate	high	
Age					
>50 years	33	6	22	5	0.214
<=50 years	68	15	46	7	
Tumor size					
T1	1	0	1	0	0.0812
T2	28	6	19	3	
T3	30	8	18	4	
T4	42	8	29	5	
Stage					
II	5	0	5	0	0.073
III	30	8	20	2	
IVa	60	12	40	8	
IVb	6	1	3	2	
Lymph node metastasis					
N0	8	0	7	1	0.5116
N1/2	64	13	44	7	
N3	29	8	17	4	

*Statistical significance was determined by the χ^2 test.

Table S2. Patient samples for Rab25 transcript analysis*, Related to Figure 2.

Tumor abbreviation	Tumor name	Normal (number)	Tumor (number)
BLCA	Bladder urothelial carcinoma	28	404
BRCA	Breast invasive carcinoma	291	1085
CESC	Cervical squamous cell carcinoma and endocervical adenocarcinoma	13	306
CHOL	Cholangio carcinoma	9	36
COAD	Colon adenocarcinoma	349	275
LUAD	Lung adenocarcinoma	347	483
LUSC	Lung squamous cell carcinoma	338	486
OV	Ovarian serous cystadenocarcinoma	88	426
PAAD	Pancreatic adenocarcinoma	171	179
PRAD	Prostate adenocarcinoma	152	492
READ	Rectum adenocarcinoma	318	92
STAD	Stomach adenocarcinoma	211	408
TGCT	Testicular germ cell tumors	165	137
THCA	Thyroid carcinoma	337	512
THYM	Thymoma	339	118
UCEC	Uterine corpus endometrial carcinoma	91	174
UCS	Uterline carcinosarcoma	78	57

* Information was from TCGA.

Transparent Methods

Cell lines

All of the radioresistant cancer cells were generated by saving the surviving residues of cells following the regimen of clinically mimic fractionated ionizing radiation (from Monday to Friday, 2Gy/day, total dose is 60 Gy) (Guo et al., 2003).Lung cancer cell lines A549, A549R, H157, H157R, H358, and H358R, were gifted from Xingming Deng (You et al., 2014). STR test was run for CNE2 and CNE2R cells. PC9 cell were bought from the cell bank of type culture collection of Chinese academy of sciences with STR authentication. Radioresistant nasopharyngeal

carcinoma cell line CNE2R (Li et al., 2013), the paclitaxel-resistant cell lines CNE1-TR and SKOV3R (Zhang et al., 2012, Hou et al., 2017, Zhou et al., 2015) were cultured following the published work. All of the cells except A549 and A549R were cultured in RPMI-1640 medium (Hyclone) with 10% FBS and 1% penicillin/streptomycin (Invitrogen, Thermo Fisher Scientific). A549 and A549R cells were cultured in DMEM/F12 medium (Hyclone) supplemented with 10% FBS and 1% penicillin/streptomycin (Invitrogen, Thermo Fisher Scientific). All cell lines were cultured at 37 °C in a 5% CO2 incubator.

Reagents and antibodies

Reagents include EGF (RD, catalog # 236-EG, 10 ng/ml) and EGF-AlexaFluor 488 (Thermofisher, catalog # E13345, 10 ng/ml, Thermofisher). The R&D Systems™ Human Phospho-Receptor Tyrosine Kinase (RTK) Array Kit (catalog # ARY001B) was purchased from R&D Company.

The following antibodies were used for western blot: anti-Rab25 from Sigma (catalog # R8532, 1:500 dilution); anti- PMCA1 (catalog # ab76020, 1: 5000 dilution), from abcam, anti-Akt, (catalog #9272, 1:1000 dilution), anti-phospho-Akt S473 (catalog#4060, 1:1000 dilution), anti-ERK1/2 (catalog#4695, 1:1000 dilution), anti-E-cadherin (catlog#14472, 1:1000 dilution), anti-N-cadherin (catlog#13116, 1:1000 dilution), anti-Vimentin (catlog#5741, 1:1000 dilution), anti-p-Tyr (catalog#8954, 1:2000 dilution), anti-phospho-EGFR (Y1068) (catalog#2234, 1:1000 dilution) and anti-phospho-ERK1/2 (catalog#4370, 1:1000 dilution), HSP90 (catalog#4877, 1:1000) from Cell Signaling; and anti-EGFR (catalog#sc-03, 1:1000

dilution), anti-GAPDH (catalog#sc-47724, 1:1000 dilution), anti-actin (catalog#sc-58673, 1:1000 dilution), and anti-Tubulin (catalog#sc-166729, 1:1000 dilution) from Santa Cruz.

The following antibodies were used for immunofluorescence and Duolink assays: anti-EGFR (catalog#ab-30, Abcam, 1:200 dilution); anti-Rab25 (catalog#HPA010872, Sigma, 1:100 dilution); and anti-EEA1 (catalog#3288, Cell Signaling, 1:100 dilution). The following antibody was used for flow cytometry: Alexa Fluor® 647 mouse anti-human EGFR (catalog#563577, BD Pharmingen, 5ul/test). The following antibody was used for IHC: anti-Rab25 from Sigma (catalog#R8532, sigma,1:100 dilution), anti-EGFR (catalog#ab-30, Abcam,1:200 dilution).

Rab25 transfection

Cells were transfected with DharmaFECT1 siRNA transfection reagent (Dharmacon) as described by the manufacturer's guidelines for 48 h. The siRNAs were generated on the basis of the following sequences: Rab25: 1# 5'-GGAAGACCAATCTACTCTC-3', and 2# 5'-TTGAGCTAGCCTTTGAGAC-3', and 3# 5'-GAACTCATTGCGCGTGAATC-3', Stat5a: 1# 5'- : GCGCTTTAGTGACTCAGAA-3', 2# 5'- ACAGAACCCTGACCATGTA-3', Stat5b: 1# 5'-ATGGGACTCAGTAGATCTT-3', 5'-GCATCACCATTGCTTGGAA-3' (Fu et al., 2019), and the control siRNA sequence was 5'-TTCTCCGAACGTGTCACGT-3'.

Construction of lentiviruses and cell transduction

Full-length Rab25 was cloned into the pLV-EF1α-MCS-IRES-Bsd lentiviral vector with a blasticidin-selectable marker (cDNA-pLV03, Biosettia). The Rab25 short hairpin RNA (shRNA) sequence (sh1# GATCCGGGAAGACCAATCTACTCTCTCAAGAGAGAGAGTAGATTGGTCTT CC TTTTTTACGCGTG, sh2#GATCCG TTGAGCTAGCCTTTGAGACTCAAGAGAGTCTCAAAGGCTAGCTCAA TTTTTTACGCGTG, sh3#GATCCGGAACTCATTGCGCGTGAATCTCAAGAGA GATTCACGCGCAATGAGTTC TTTTTTACGCGTG) and the control shRNA sequence (GATCCG TTCTCCGAACGTGTCACGTTCAAGAGAACGTGACACGTTCGGAGAA TTTTTTACGCGTG) were cloned into Lenti-X™ shRNA Expression Systems (Clontech) with a puromycin-selectable marker. The Gag-Pol + Rev expression vector and VSV-G expression vector packaging plasmids were co-transfected with the pLV-EF1α-MCS-IRES-Bsd-Rab25 construct or the shRab25 construct in HEK293T cells for 48 h according to the manufacturer's instructions. The virus was collected 48 h after transfection, and cells were selected with blasticidin (8 μg/ml) or puromycin (1 μg/ml), respectively.

Immunoblotting

Cells were harvested and lysed in RIPA buffer plus protease inhibitor cocktail and phosphatase inhibitor cocktail (Selleck). The protein samples were separated by SDS-PAGE under reducing conditions and transferred onto polyvinylidene difluoride (PVDF) membranes (0.22 and 0.45 μm, Millipore, Bedford, MA, USA).

Subsequently, the membrane was blocked with 5% skim milk in TBST buffer (TBS containing 0.1% Tween-20) for 1 h at room temperature and then hybridized with primary antibody with gentle agitation overnight at 4°C. After being washed with TBST three times, the membrane was incubated with HRP-conjugated secondary antibody (Santa Cruz) for 1 h at room temperature. Bands were detected with a Pierce ECL Western Blotting Substrate detection system (Thermo Scientific) and visualized using a Gel Doc™ XR+ System (Bio-Rad). Three independent experiments were performed.

RNA extraction and real-time quantitative PCR

Total RNA was extracted from cells according to the manufacturer's protocol using TRIzol reagent (Invitrogen). The dissolved RNA sample was measured on a spectrophotometer to determine the concentration and quality before being converted to complementary DNA (cDNA). RNA samples were reverse transcribed using a SuperScript III First-Strand Synthesis SuperMix for qPCR Kit (Life Technologies, California, USA), and quantitative real-time PCR (qRT-PCR) analysis was performed using a CFX-96 Real-time PCR System (Bio-Rad, Hercules, CA, USA). The values were expressed as fold changes compared with the corresponding values for the control using the $2^{-\Delta\Delta Ct}$ method.

PCR array analysis

Quantitative RT-PCR for cell death-associated genes was performed using a Cell Death Pathway Finder PCR Array (PAHS-212Z, QIAGEN, MD, USA) according to the manufacturer's protocol. For data analysis, a web-based software from data

analysis center of QIAGEN was used. The fold-changes were then calculated and expressed as log-normalized ratios of the values from the CNE2R cells to those of the CNE2 cells.

Tumor xenografts and radiotherapy

All of the animal experiments were approved by the Animal Ethics Committee of Xiangya Hospital Central South University and followed the Guidelines of Animal Handling and Care of Central South University. The BALB/c nude mice used in our animal model were 4- to 6-week-old female mice. Cells ($5x10^5$ cells/mouse) stably transduced with or without the Rab25 shRNA lentivirus were suspended in 100 μl of RPMI-1640 medium mixed with Matrigel (1:1) and injected subcutaneously into the left flank of the mice for NPC or lung cancer tumor formation. Tumor growth was recorded every other day with a caliper according to the following formula: tumor volume = the shortest diameter^2 × the largest diameter × 0.5. After the tumors reached a volume of approximately 200 mm^3, the irradiation treatment groups were irradiated with 2 Gy locally at the tumor every two days, for a total dose of 4 Gy.

For establishment of radio-insensitive NPC xenografts, CNE2 cells ($5x10^5$ cells/mouse) were injected subcutaneously into the left flank of the mice for NPC tumor formation (named P0 mice). When the tumors reached a volume of approximately 200 mm^3, tumor tissues were harvested and divided into equally sized pieces (volume of 1-2 mm^3) immediately after removal from the mouse. Approximately 5-6 tumor pieces were then inoculated subcutaneously into the left flank of recipient mice for tumor formation (named P1 mice); the remaining tissue

was fixed in 10% formalin for IHC analysis. An X-ray treatment of 5 Gy was administered locally to the tumor for two days when the tumor volume of the P1 mice reached 200 mm^3. After 5 days of treatment, the mice were sacrificed, and the tumors were immediately cut into small pieces for inoculation into the left subcutaneous flank of recipient mice for tumor formation (named P2 mice). When the tumor pieces had been transferred to the P11 mice, we compared the growth rate of tumors between P2 and P11 mice. Data are presented as the tumor volume (n=4, Mean ± SD, *$p<0.05$). Statistical analysis was performed using the Student's t test and the software Graphpad Prism.

Immunohistochemistry

Paraffin-embedded slides were incubated at 70°C for 90 min and then deparaffinized with xylene and rehydrated. Endogenous peroxidase activity was quenched with 3% H_2O_2 solution for 15 min at 37°C, and antigen retrieval was performed in a pressure cooker using sodium citrate buffer (10 mM, pH 6.0). Sections were immuno-stained with antibodies against Rab25 and EGFR. All immunostainings were performed with the avidin-biotin-peroxidase complex technique in combination with diaminobenzidine (DAB), and the slides were counterstained with hematoxylin and eosin (H&E) for surgical pathology specimens. The use of NPC patient tumor samples in this study was approved by the Human Ethical Committee of Xiangya Hospital of Central South University.

The immunoreactive proteins in the tissue were evaluated with scores based on the proportion of positive tumor cells. Random 3-5 sections of each sample and 5-6

high-power fields (HPF) of each section were used for analysis and quantification. Fields with different staining intensity were counted separately when the staining was not homogeneous. According to the IHC staining intensity, the following criteria were used for interpretation of IHC data. High expression was defined as strong staining intensity in more than 75% of tumor cells (score=4); medium expression was moderate staining intensity in more than 50% of tumor cells (score=3); low expression was weak staining intensity in more than 25% of tumor cells (score=2); negative expression was weak staining in less than 25% of tumor cells (score=0-1).

Immunofluorescence

Cells were quickly rinsed with pre-warmed PBS and fixed with 4% paraformaldehyde (PFA) in PBS for 20 min at 37°C, permeabilized in 0.5% Triton X-100 for 20 min and blocked with BlockAid^{TM} blocking solution (Thermo Fisher) for 1 h. After labeling with primary antibodies overnight at 4°C, cells were washed in PBS and incubated with Alexa Fluor-conjugated secondary antibodies for 45 min at room temperature. All antibody incubations were performed in BlockAid^{TM} blocking solution. The coverslips were mounted with DABCO anti-fade agent on glass slides and imaged using DeltaVision OMX SR (GE) equipped with a 63x/1.4 numerical aperture oil-immersion objective. For quantification of the EGFR internalization in early and late endosomes or to evaluate the co-localization of EGFR and Rab25, the software MetaMorph was used to analyze the co-localization of signals from the Rab25 and EEA1 channels.

Immunoprecipitation

Cells were fixed with 4% PFA for 15 min and lysed in RIPA buffer. Protein A/G magnetic beads were first suspended in binding buffer (50 mM Tris, 150 mM NaCl, 0.1%-0.5% Triton 100 or Tween 20, pH 7.5) and then incubated with 5 μg Rab25 antibody or normal rabbit IgG antibody for 1 h at room temperature with end-over-end rotation. After the supernatant was removed, 200 mg of cell lysate was added to each tube, which was incubated with rotation for 10 min at room temperature. The immunoprecipitated proteins were released by boiling for 5 min at 95°C in SDS–PAGE sample buffer. The magnetic beads were removed with a magnetic separator before the samples were loaded onto a 12% SDS–PAGE gel.

Duolink proximity ligation assay

The in situ proximity ligation assay was performed using a Duolink® In Situ Red Starter Kit for Mouse/Rabbit (DUO92101, Sigma) according to the manufacturer's instructions. Briefly, cells were seeded onto coverslips and circled with a hydrophobic pen the day before the experiment. After treatment, the cells were fixed, permeabilized, blocked, and then incubated with primary antibodies at 4°C overnight. After washing, the oligonucleotide (Minus and Plus)-conjugated secondary antibodies were added and incubated for another hour at 37°C. Subsequently, cells were washed and incubated with ligation solution for 30 min at 37°C. The ligated nucleotide circles were amplified using polymerase via the addition of amplification solution and incubation for 100 min at 37°C. The slides were washed briefly, and Duolink® In Situ Mounting Medium with DAPI (DUO82040, Sigma) was added to each sample to

stain cell nuclei for fluorescence microscopy. The visualized fluorescence spots represented the clusters of protein-protein interactions.

EGF uptake and EGFR internalization assay

Cells were serum-starved for 6 hours and used for either EGF uptake or EGFR internalization assays. For the quantitative EGF uptake assay, cells were treated with 1 ng/ml or 100 ng/ml EGF-Alexa488 (Invitrogen) for the indicated time at 37°C. For the EGFR internalization assay, cells were treated with 1 ng/ml EGF (RD) for the indicated time at 37°C. A plate incubated in RPMI-1640 medium without ligand for 30 min or 180 min was used as a control. EGF uptake was halted by placing the cells on ice followed by two washes in ice-cold phosphate-buffered saline (PBS). To remove surface-bound EGF, cells were washed three times for 5 min each with cold acid buffer (RPMI-1640/0.2% BSA, pH 3.5 adjusted with HCl). The 'pulse-chase' assay was conducted as previously described (Kondapalli et al., 2015). Cells were treated 1 ng/ml EGF for 30 min and then transferred to ice to halt EGFR internalization. After three washes with cold acid buffer, the plates used for observing the EGFR recycling process were cultured in RPMI 1640 with glutamine (Hyclone) in an incubator at 37°C and 5% CO_2 for the indicated time. The EGFR recycling process was halted by transferred the plates to ice. For the quantitative EGF uptake assay, cells were detached from the culture dishes, centrifuged at 300 ×g for 5 min at 4°C and suspended in 0.2% BSA in PBS. For the EGFR internalization assay, cells were detached and incubated with Alexa 647-EGFR antibody in PBS for 20 min. After washing once with 0.2% BSA in PBS, cells were fixed in 4% PFA in PBS. Flow

cytometry was performed using a Millipore Guava® easyCyte HT Sampling Flow Cytometer.

Flow cytometry analysis of anoikis and apoptosis

An anoikis resistance assay was performed by seeding cells in a 6-well ultra-low attachment surface polystyrene culture dish (Corning 3473) using regular culture medium. For cell apoptosis analysis, the cells were collected at different time points and resuspended in Annexin V binding buffer supplemented with Annexin V and propidium iodide (Roche). Anoikis was quantitated by flow cytometry, and the degree of apoptotic cell death (%) was determined by flow cytometry (Millipore) using Annexin V-FITC/PI staining.

Colony-forming assay

Cells were seeded at a density of approximately 200 cells per well in six-well plates and irradiated with various doses 24 h after plating. The cells were then cultured for 12 days to allow colony formation. Only the single clones that contained more than 50 cells were counted. During colony growth, the culture medium was replaced every 3 days. Each treatment was performed in triplicate.

Tumor sphere formation assay

Single-cell suspensions were seeded into 6-well ultra-low attachment surface polystyrene culture dish (Corning 3473) at a density of 500 cells/ml. Cells were grown in serum-free medium, supplemented with B27 (Life Technology), 20 ng/ml EGF (Biovision), 20 ng/ml basic-FGF, and 4 μg/ml heparin (VWR). Cells were cultured for 10 days and tumor spheres were counted, sphere size were measured and

calculated under light microscopy and collected for further experiments. Three independent experiments were done in triplicate.

Kaplan-Meier survival analyses

TCGA RNA-seq data for LUAD samples were obtained from UCSC Xena browser (http://xena.ucsc.edu/). The overall survival or disease-free survival of LUAD patients were evaluated using the Kaplan–Meier method, and statistical differences in survival times were determined using the log-rank test as described elsewhere. The cohort include 720 lung adenocarcinoma samples obtained from Kaplan-Meier Plotter (http://kmplot.com/analysis/index.php?p=service&cancer=lung) were used to generate the overall survival analyses of LUAD patient based on Rab25 (Affy ID, 218186_at) status. Patients were split by median expression of Rab25. The cohort include 478 LUAD samples were obtained and analysis by GEPIA website for disease free survival analysis. A log rank test was used to test for differences of more than one survival curve.

Quantification and statistical analysis

Data was presents as mean ± standard deviation (SD). GraphPad Prism was used for statistical analysis. ANOVA analysis was used for comparison study of more than two data groups and student's t-test was used to compare two groups of independent samples. Pearson correlation test was utilized to evaluate the association of staining intensities of EGFR and Rab25 in NPC patients who received radiotherapy. Image J was used to quantified and normalized data. Significance was indicated as follow: NS, not significant; * $p<0.05$; ** $p<0.01$.